

Cross-Forming Control and Fault Current Limiting for Grid-Forming Inverters

Xiuqiang He, *Member, IEEE*, Maitraya Avadhut Desai,
Linbin Huang, *Member, IEEE*, and Florian Dörfler, *Senior Member, IEEE*

Abstract—We propose a novel “cross-forming” control concept for grid-forming inverters operating against grid faults. Cross-forming refers to *voltage angle forming* and *current magnitude forming*, differing from classical grid-forming and grid-following concepts, i.e., voltage magnitude-and-angle forming and current magnitude-and-angle forming, respectively. Unlike purely grid-forming or grid-following paradigms, the cross-forming concept is motivated by device security requirements for fault current limitation and meanwhile grid code requirements for voltage angle forming preserving. We propose two feasible cross-forming control implementations, enabling inverters to quickly limit fault currents at a prescribed level and preserve voltage angle forming for grid-forming synchronization and dynamic ancillary services provision, during symmetrical or asymmetrical fault ride-through. Moreover, the cross-forming control yields an equivalent system featuring a constant virtual impedance and a “normal form” of representation, allowing us to extend previously established transient stability results to encompass scenarios of current saturation. Simulations and hardware experiments validate the efficacy of the proposed cross-forming control.

Index Terms—Current limiting, fault ride-through (FRT), grid faults, grid-forming inverters, overcurrent, transient stability.

I. INTRODUCTION

GRID-forming inverters play a crucial role in future power systems in autonomously regulating grid frequency and voltage. While a grid-forming inverter operates like a voltage source, limiting its current during grid disturbances is vital to avert potential overcurrent damage. Moreover, grid-forming inverters should sustain transient stability during grid faults, i.e., ensuring synchronization while transitioning from one operating state to another. The transient stability is crucial for successful fault ride-through (FRT) and ancillary services provision during FRT, e.g., fault current injection and phase jump power provision, performance requirements of grid codes, see Great Britain and Australian grid codes [1], [2] or a survey in [3]. To satisfy these requirements, grid-forming inverters should maintain grid-forming synchronization and supply FRT ancillary services as continuously as possible, even when the current reaches the limit [1]–[3]. These requirements involve technical challenges in limiting fault current, maintaining transient stability (synchronization), and providing FRT ancillary services simultaneously.

A. Related Work

When grid-forming inverters operate without current saturation within normal grid conditions, managing grid-forming

synchronization and providing grid-forming ancillary services is more straightforward. In respect thereof, the transient stability of grid-forming inverters has been widely investigated in the literature, refer to [4] for a comparative study and [5], [6] for a review. In parallel, the dynamic ancillary services provision of grid-forming inverters within normal operating conditions has also been extensively explored in the literature, see [7] for a survey. In contrast to normal operating conditions, the critical challenge under grid fault conditions arises from current limiting. In the literature, the current limiting of grid-forming inverters is typically addressed with three strategies: 1) Adaptive/threshold virtual impedance [8], [9]; 2) Current limiter cascaded with virtual admittance [10]–[14]; and 3) Current-forming voltage-following control [15]–[21]. These strategies have different merits and demerits as follows.

1) *Adaptive/Threshold Virtual Impedance*: This strategy uses current feedback to increase the virtual impedance magnitude adaptively, thus declining the voltage reference and ultimately reducing the overcurrent [8], [9]. The strategy can preserve the original grid-forming synchronization and ancillary services provision. However, the parameter tuning thereof is quite complicated due to the consideration of the worst case to ensure reliable current limiting [8] and the concerns of small-signal and transient stability performance [22]. In most cases, the strategy underutilizes the overcurrent capability due to the inherent characteristics of proportional feedback. Moreover, the equivalent virtual impedance varies with state-dependent overcurrent severity, distorting the power output characteristics [23], [24] and thus complicating transient stability analysis.

2) *Current Limiter Cascaded With Virtual Admittance*: This strategy uses a virtual admittance to act as a voltage proportional regulator [12]–[14], avoiding limiter-induced windup issues inherent in integrator-included regulators (e.g., classical PI regulators), and meanwhile preserving grid-forming synchronization and ancillary services provision. This strategy is simple to implement, easy to tune, and fully utilizes the overcurrent capability. However, current saturation still leads to a varying equivalent impedance [12], [13], similar to the virtual impedance strategy. Likewise, the varying impedance distorts the power-angle characteristics (from an ideal sine function to a complex nonlinear one) [11]–[14], making transient stability studies analytically intractable.

3) *Saturated Current-Forming Control*: This strategy deactivates the voltage control loop during current saturation while preserving the current control [15]–[19], with the reference angle of the current vector control generated by a power-frequency droop control. This strategy falls into the category of current-forming controls [25] since the controlled variable

X. He, L. Huang, and F. Dörfler are with the Automatic Control Laboratory, ETH Zurich, 8092 Zurich, Switzerland. M.A. Desai is with the Power System Laboratory, ETH Zurich, 8092 Zurich, Switzerland. Emails: xiuqhe@ethz.ch, linhuang@ethz.ch, dorfler@ethz.ch, desai@eeh.ee.ethz.ch.

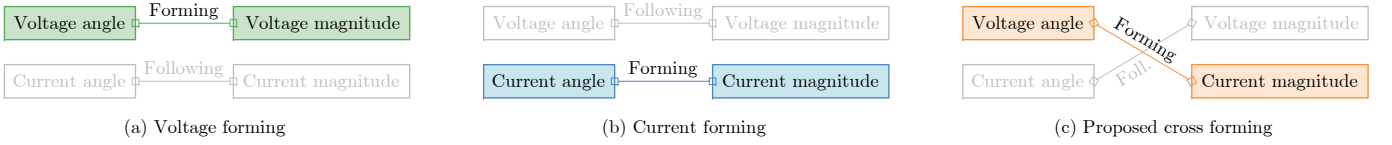


Fig. 1. Illustrations of voltage-forming, current-forming, and cross-forming behaviors in different forming control concepts.

under forming is current rather than voltage. Hence, while effective for current limiting, this strategy cannot independently provide voltage-forming behaviors and services.

Concisely, the current-limiting prior arts are affected by multiple demerits, rendering them insufficient for fulfilling the requirements for current limiting, transient stability guarantees, and grid-forming ancillary services during FRT.

B. Motivations

We aim to develop a new control concept, termed cross-forming, to address the fault current limiting of grid-forming inverters. The cross-forming concept refers to voltage angle forming and current magnitude forming, which is motivated by the following three facts/observations. First, preserving voltage angle forming is essential for achieving grid-forming synchronization and frequency-/angle-sensitive ancillary services, e.g., phase jump *active power* provision and fault *reactive current* injection [1], [2]. Second, the magnitude of the inverter terminal voltage during current saturation proves to passively follow the grid operation, called “voltage decline” in [26], rendering voltage magnitude forming unnecessary in such scenarios. Third, the current-limiting constraint suggests that current magnitude forming is required. These facts/observations motivate us to enforce voltage angle forming and current magnitude forming, exhibiting cross-forming behaviors during current saturation, as illustrated in Fig. 1. The cross-forming behaviors prove to satisfy the previous requirements sufficiently.

C. Contributions

The contributions of this paper are summarized as follows:

- Considering voltage angle forming required, voltage magnitude forming lost, while current magnitude limiting required, we present the concept of cross-forming control and show that it naturally achieves current limiting, grid-forming synchronization, FRT services provision, etc.
- We develop two feasible cross-forming control implementations, both of which apply to symmetrical and asymmetrical grid fault conditions. The cross-forming control yields an equivalent circuit featuring a constant virtual impedance, differing from prior results.
- Based on the equivalent circuit, we present an equivalent representation of the cross-forming inverter, which conforms to the normal form of current-unsaturated grid-forming systems. Hence, existing transient stability analysis approaches and results for current unsaturation are readily extended to current-saturated conditions.
- As a side contribution, we provide a survey of prior arts in Appendices, including grid-forming controls, negative-sequence controls, and typical current-limiting strategies,

facilitating the understanding of this work, stimulating further research of grid-forming technologies, and offering useful references for practical applications.

We highlight that the proposed cross-forming control is fast-acting, able to fully utilize the overcurrent capability, adaptable to various disturbances, simple to implement, easy to tune, and robust in stability performance, therefore serving as a promising candidate for future grid-forming product development.

D. Organization and Notation

The remainder of the paper is organized as follows. Section II outlines grid-forming control objectives against grid faults, defines the cross-forming concept, and discusses its capabilities to serve grid code requirements. Section III presents the cross-forming control design and a comparison with existing strategies. Section IV derives the equivalent normal form and extends the prior transient stability results. Simulation and experimental validations are provided in Section V. Section VI concludes the paper. Finally, the review of relevant prior arts is provided in Appendices A to C.

Notation: We use $\underline{v} := v_\alpha + jv_\beta$ and $\underline{i} := i_\alpha + ji_\beta$ to denote voltage and current vectors in the stationary reference frame, respectively, and $\underline{v}_{dq} := v_d + jv_q$ and $\underline{i}_{dq} := i_d + ji_q$ to denote voltage and current vectors in the rotational reference frame, respectively. The underlines throughout the paper indicate complex variables. $\text{Re}\{\cdot\}$, $\text{Im}\{\cdot\}$, $|\cdot|$, and $\angle(\cdot)$ denote the real part, the imaginary part, the modulus and the angle of a complex number, respectively, and $\text{conj}(\cdot)$ denote the associated complex conjugate. Superscripts $+$ and $-$ indicate positive- and negative-sequence components, respectively.

II. GRID-FORMING CONTROL OBJECTIVES, OPERATION MODES, AND FRT SERVICES PROVISION

The aim of this section is three-fold. We first outline grid-forming control objectives under grid faults from the perspective of stability and grid code requirements. Then, we define and categorize typical operation modes of power inverters, and finally, we investigate their FRT services provision capabilities under current saturation to achieve the control objectives.

A. Grid-Forming Control Objectives Under Grid Faults

The control objectives of grid-forming inverters under grid faults should ideally remain the same as under normal conditions. However, grid-forming inverters must limit their output current to prevent overcurrent damage. Moreover, under asymmetrical grid faults, the control of negative-sequence components should also be of concern. We summarize the grid-forming control objectives under grid faults in the following.

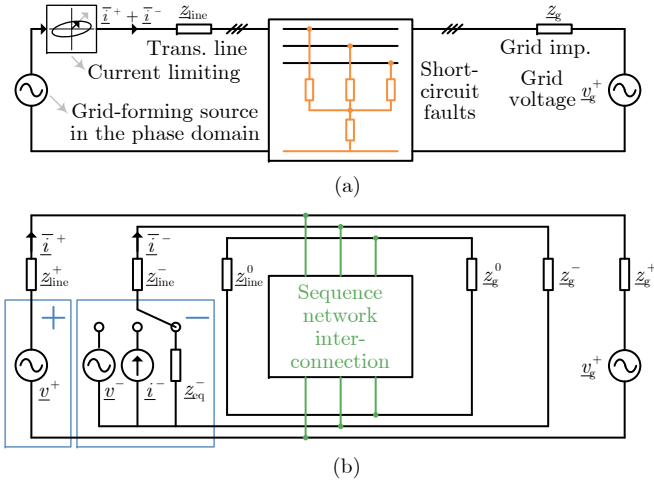


Fig. 2. (a) Phase-domain and (b) sequence-domain generic equivalent circuit for grid-forming inverters under grid short-circuit faults, where the grid-forming operation is maintained in the positive sequence while the negative sequence admits different options among negative-sequence grid-forming [27], current injection [28], or impedance emulation [29].

1) *Grid-Forming Synchronization*: Synchronization of angular frequency is a necessary condition for closed-loop control and stability, typically achieved by grid-forming-type feedback control (i.e., grid-forming synchronization).

2) *Positive-Sequence FRT Services Provision*: The regular dynamic ancillary services under normal grid conditions typically include frequency and voltage regulation. Concerning grid faults, grid-forming devices are required by grid codes to maintain a constant internal voltage phasor in a short time frame and to be able to rapidly supply fault (reactive) current or phase jump (active) power after grid voltage dips or phase jumps, respectively [1], [2] (for instance, as specified in the GB grid code [1], with an initial delay less than 5 ms and full activation time less than 30 ms).

3) *Negative-Sequence FRT Services Provision*: In Fig. 2, we show generic equivalent circuits in the phase domain and the sequence domain under asymmetrical grid faults. The FRT services in the negative-sequence domain are also of concern, which typically admit multiple options, depending on specific requirements. The options include: i) Negative-sequence grid-forming (behaving as a voltage source) symmetric to the positive-sequence grid-forming [27]; ii) Negative-sequence current injection (behaving as a current source) for power oscillation suppression [28]; iii) Negative-sequence voltage mitigation [29] (behaving as a virtual impedance), a requirement of grid codes, see IEEE Std. 2800 [30]).

4) *Current Limiting*: The current limit of the inverters must be respected regardless of the control objectives or strategies used. This requires that the maximum phase current magnitude remains within or at the limit. Moreover, voltage limits preventing overmodulation are also of concern in practice, which is more of a concern for high-/over-voltage ride-through.

B. Forming Control Modes

We introduce three types of forming control modes, as displayed in Fig. 1. The first two modes are well known, while

the last is novel and it inspires new solutions to address current limiting and transient stability challenges in grid-forming inverters under grid faults.

Definition 1. Voltage-Forming (Current-Following) Mode: A voltage-source mode whose voltage phase-angle and magnitude are independently controlled and whose current depends on an external grid circuit, as illustrated in Fig. 1(a).

Definition 2. Current-Forming (Voltage-Following) Mode: A current-source mode whose current phase-angle and magnitude are independently controlled and whose voltage depends on an external grid circuit, as illustrated in Fig. 1(b).

Definition 3. Cross-Forming Mode: A hybrid source whose voltage phase-angle and current magnitude are independently controlled and whose voltage magnitude and current phase-angle depend on an external circuit, as illustrated in Fig. 1(c).

Since power systems provide voltage source behaviors, the concept of grid-forming (GFM) and grid-following (GFL) is more precisely *voltage-forming* and *voltage-following*, respectively [25]. In particular, a voltage-forming source and a current-forming source share a dual relationship [25]. Voltage-forming control modes typically include droop control, virtual synchronous machine (VSM), and dispatchable virtual oscillator control (dVOC), with forming characteristics in voltage angle and magnitude. In contrast, current-forming modes feature forming characteristics in current angle and magnitude. Typical examples include phase-locked loop (PLL)-based current control and the control schemes that are structurally dual to droop control and VSM [20], [25].

The control objectives outlined in Section II-A require us to enforce both current limiting (necessary) and voltage forming (as far as possible) under grid faults. The objectives cannot be achieved simply using either voltage-forming mode or current-forming mode, since the former requires additional remedies to limit current, while the latter is opposed to voltage-forming. To inherently fulfill the control objectives, we propose the concept of cross-forming in Definition 3. The cross-forming mode features the *voltage-angle-forming* and *current-magnitude-forming* characteristics, therefore preserving the voltage-angle-forming capability and enabling an inherent current-magnitude-limiting capability. The *voltage-magnitude-forming* capability, established under normal operating conditions, is lost as a result of current saturation [26]. This finding is formulated and proved in Proposition 1.

Proposition 1. Voltage Magnitude Following Under Current Saturation: Consider the circuit in Fig. 3(a). Given that the current magnitude $|i|$ of the inverter is saturated (it can therefore only be a current-forming source or a cross-forming source). Assume that the circuit allows a steady state. The voltage magnitude $|v|$ of the inverter terminal in steady state is determined by the given conditions, i.e., it cannot be exclusively specified by the source itself.

Proof: The proof for the case of a current-forming source is trivial, since the voltage is determined by the output current and the external circuit, see Fig. 3(b), where the voltage drop on the grid impedance is determined as $\Delta v_z = i z_g$. In the

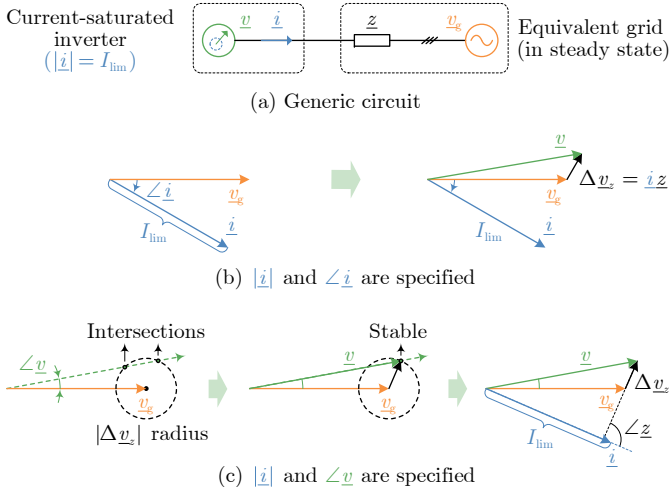


Fig. 3. (a) A generic circuit representing a current-saturated inverter ($|\underline{i}| = I_{lim}$) connected to a grid. In both (b) and (c), where $\angle \underline{i}$ and $\angle \underline{v}$ are specified, respectively, the voltage magnitude $|\underline{v}|$ passively follows the circuit law.

case of a cross-forming source, since the current magnitude is specified, $|\Delta \underline{v}_z| = |\underline{i} \underline{z}|$ is constant. Consider the circuit law in the steady state,

$$\underline{v} = \underline{v}_g + \Delta \underline{v}_z = \underline{v}_g + \underline{i} \underline{z}. \quad (1)$$

If the circuit allows a steady state, we can see from Fig. 3(c) that the green arrow indicating the specified $\angle \underline{v}$ must cross the dashed circle which has a radius $|\Delta \underline{v}_z|$ and is centered at the vertex of \underline{v}_g . This would imply that there exists \underline{v} to satisfy (1). In addition, the direction of \underline{i} results from $\Delta \underline{v}_z$. There may exist two intersections, between which the one with a larger voltage magnitude (corresponding to inductive reactive current provision) proves to be stable and the other is unstable, depending on a specific control, see Section III later. For either intersection, the voltage \underline{v} of the source follows from the given conditions. Hence, it cannot be specified by the source. ■

Proposition 1 reveals that for a current-saturated voltage-forming inverter (irrespective of the control method used), the terminal voltage magnitude can no longer be controlled independently. In other words, a current-saturated voltage-forming inverter loses the ability to impose the terminal voltage and instead exhibits a voltage magnitude-following behavior to respect the circuit law. However, the fact that the voltage magnitude follows does not imply a great challenge for grid-forming inverters to satisfy the requirements of FRT services. This is because the service in terms of low-voltage ride-through focuses on fault current provision instead of voltage magnitude maintenance. Moreover, even if the voltage-magnitude-forming capability is lost, the voltage-angle-forming capability can still be preserved. This is crucial to provide an autonomous voltage angle reference for the reactive fault current provision during low-voltage ride-through and active phase jump power provision during phase jump ride-through or active inertia power provision during frequency drifts, as required in grid codes [1], [2]. It is important to note that Proposition 1 can be extended to unbalanced grid fault conditions. Briefly, the Thevenin equivalent grid in Fig. 3(a) can be obtained in the

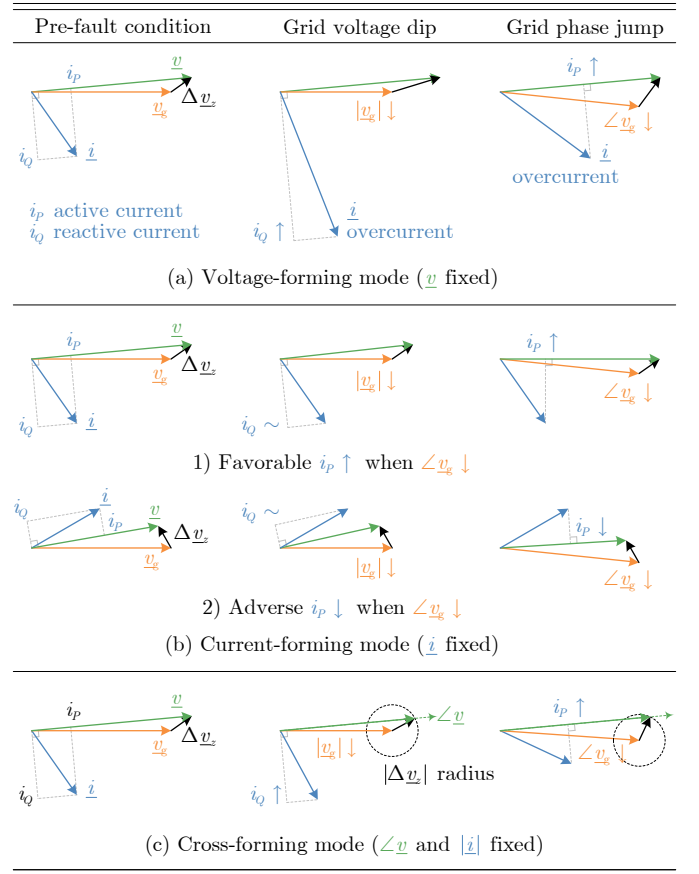


Fig. 4. Provision of fault reactive current i_Q and phase jump active current i_P under a grid voltage dip and phase jump, respectively, where the variables under forming are considered unchanged at the moment of disturbances.

positive-sequence domain by aggregating the rest of the components in the sequence-domain circuit [31].

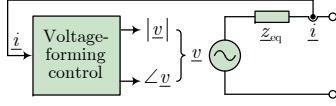
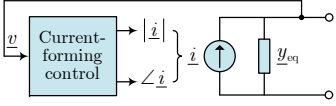
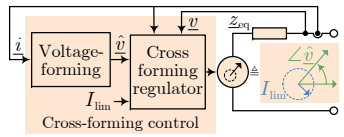
C. FRT Services Provision Capabilities

The comparison of the three operation modes is provided in Table I. The FRT services provision capabilities discussed in this subsection include fast fault current injection and phase jump power supply, apart from current-limiting capabilities.

Voltage-Forming Mode: This mode can naturally provide fault (reactive) current injection and phase jump (active) power as it acts as a voltage-forming source. This is illustrated in Fig. 4(a). The reactive current i_Q increases naturally when the grid voltage dips, providing a fast reactive current to counteract the voltage dip. The active current i_P increases naturally when the grid phase jumps backward, providing fast active power to counteract the phase jump. Since the voltage-forming mode requires the output current to naturally respond to disturbances, it does not provide any current-limiting capabilities on its own. Numerous remedies have been developed to address the current-limiting challenge; see Appendix C for a review.

Current-Forming Mode: The response of a converter operating in this mode to a voltage dip or phase jump is depicted in Fig. 4(b). Inherently, this mode does not provide any voltage-forming capabilities. When the grid voltage dips, if the current reference is fixed, the reactive current i_Q will remain almost

TABLE I
THREE FORMING CONTROL MODES, CHARACTERISTICS, AND REGULAR AND FRT SERVICES PROVISION CAPABILITIES

	Voltage-forming mode	Current-forming mode	Cross-forming mode
Illustrations			
Examples	Droop, VSM, dVOC, and complex droop control ¹	PLL-based current control, and the dual of droop/VSM	Two types, see Section III
References	[5]	[15], [32]	This work
Voltage behavior	Angle and magnitude forming	Angle and magnitude following	Angle forming, magnitude following
Current behavior	Angle and magnitude following	Angle and magnitude forming	Angle following, magnitude forming
Synchronization	Voltage angular frequency	Current angular frequency	Voltage angular frequency
Regular services	Voltage magnitude-frequency control	Current magnitude-frequency control	Voltage frequency and current magnitude control
Fault current	Yes, natural response, favorable	Yes, via setpoint adjust	Yes, natural response, favorable
Phase jump power	Yes, natural response, favorable	Yes, but typically adverse	Yes, natural response, favorable
Neg.-seq. services ²	Yes, flexible	Yes, flexible	Yes, flexible
Current limiting	No, additional remedies required ³	Yes, inherent	Yes, inherent

¹ A review of grid-forming controls is provided in Appendix A.

² A review and rigorous proofs of multiple control modes for negative-sequence components are presented in Appendix B.

³ A categorized review of typical existing current-limiting strategies for voltage-forming control mode is presented in Appendix C.

the same as the pre-fault condition (assuming that the current-forming is also used before the fault). To provide a required reactive current, one needs to adjust the current reference [20], [21]. When the grid phase jumps, the active current i_P may increase or decrease, i.e., the change of i_P can be favorable or adverse, depending on the pre-fault operation state. Likewise, one needs to adjust the current reference to ensure a favorable active power provision [21]. The merit of the current-forming mode lies in its inherent current-limiting capability.

Cross-Forming Mode: Since the voltage angle in the cross-forming mode is autonomously controlled, this control mode provides additional reactive current i_Q when the grid voltage dips and offers favorable phase jump active current i_P when the grid phase jumps, as shown in Fig. 4(c). Therefore, the voltage-angle-forming characteristics enable the capabilities of fast fault current injection and phase jump power provision. Meanwhile, the current-magnitude-forming characteristics allow for inherent current limiting. It is noted that the provision of i_Q and i_P is not as large as in the voltage-forming mode, since the current magnitude is fixed in the cross-forming mode.

Regarding negative-sequence services under asymmetrical grid faults, typical requirements include twice-fundamental-frequency power oscillation suppression [33] or voltage imbalance mitigation [30]. Since the control of negative-sequence components can be readily implemented, see Appendix B, the achievement of negative-sequence services is not challenging, remaining flexible for all three control modes.

III. CROSS-FORMING CONTROL

In this section, we develop feasible implementations of the cross-forming mode. We first present a desired equivalent circuit which is then used to design the control implementations.

A. Desired Equivalent Circuit of Cross-Forming Mode

A desired equivalent circuit of the cross-forming control is shown in Fig. 5, where the output current has a specified

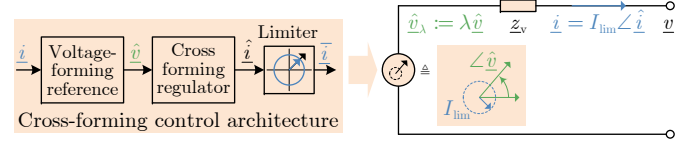


Fig. 5. A desired equivalent circuit for grid-forming inverters operating under current saturation, where the cross-forming control performs voltage-angle-forming and current-magnitude-forming behaviors.

magnitude I_{lim} and the virtual internal voltage has a specified angle $\angle \hat{v}_\lambda$. Moreover, a virtual impedance \underline{z}_v (constant) can be added to enhance control flexibility and performance. Given that the magnitude of the virtual internal voltage cannot be exclusively specified by the source itself (cf. Proposition 1) and that the virtual internal voltage is required to have the same angle as $\angle \hat{v}$ to preserve voltage angle forming, we denote the virtual internal voltage of the desired circuit in Fig. 5 as

$$\hat{v}_\lambda := \lambda \hat{v}, \quad (2)$$

where $\lambda \in \mathbb{R}_{>0}$ denotes the ratio between the virtual internal voltage \hat{v}_λ and the reference voltage \hat{v} . We note again that by Proposition 1, $|\hat{v}_\lambda|$ and further λ follow the circuit law. The voltage equation of the desired equivalent circuit in Fig. 5 is given as

$$\hat{v}_\lambda = \lambda \hat{v} = \underline{v} + \underline{z}_v \underline{i}, \quad |\underline{i}| = I_{lim}, \quad (3)$$

which indicates that, on the one hand, the voltage angle forming is preserved in the virtual internal voltage, and on the other hand, the current-limiting behavior is enforced.

Remark 1. Differences From Prior Equivalent Circuits: We highlight that the equivalent circuit proposed in this work differs from previous results in the literature. Typically, prior results that address current limitations use an adaptive virtual impedance or a current limiter along with a virtual admittance (see the review in Appendix C for additional details). For these strategies, a variable (specifically, current-dependent)

virtual impedance is obtained in the equivalent circuits. Using the cross-forming control proposed, the virtual impedance in our circuit remains constant while the virtual internal voltage magnitude follows the response of the external circuit. This allows us to obtain an equivalent power network and recover an *equivalent normal/canonical form* like the normal form of voltage-forming systems. Hence, our equivalent circuit facilitates transient stability analysis since we can extend existing transient stability results from current-unsaturated to current-saturated conditions, a benefit that remains unestablished with previous current-limiting strategies.

B. Cross-Forming Control Design

Next, we present viable control implementations to ensure that inverters fulfill the desired voltage equation in (3). As shown in the generic diagram in Fig. 5, the control architecture comprises three modules. The standard voltage-forming reference module aims to provide a voltage-forming reference \hat{v} and is embodied as part of the cross-forming control architecture. Similarly, the current limiter is also a separate standard module. The novel cross-forming regulator module takes the voltage reference \hat{v} to generate a current reference \hat{i} . This regulator aims to match the angle of the virtual internal voltage angle with the angle of the voltage reference, i.e., $\angle \hat{v}_\lambda = \angle \hat{v}$. The cross-forming regulator thus differs from the classical voltage-tracking controller.

To facilitate the design of the cross-forming regulator, we rewrite the desired circuit equation in (3) as

$$\hat{i} = \frac{1}{z_v} (\hat{v}_\lambda - \underline{v}). \quad (4)$$

We further define the degree of saturation (DoS, also known as current-limiting factor [34]) as the ratio between the saturated current reference $\bar{\hat{i}}$ and the unsaturated current reference \hat{i} , i.e.,

$$\text{DoS (balanced): } \mu := \frac{\bar{\hat{i}}}{\hat{i}} \stackrel{(\text{saturated})}{=} \frac{I_{\text{lim}}}{|\hat{i}|}, \quad (5)$$

where $\mu \in (0, 1]$. Based on the definition of μ and assuming that the output current \hat{i} tracks the saturated current reference $\bar{\hat{i}}$, i.e., $\hat{i} = \bar{\hat{i}}$, the circuit equation in (4) is reformulated as

$$\hat{i} = \frac{1}{z_v} \left(\frac{\hat{v}_\lambda}{\mu} - \frac{\underline{v}}{\mu} \right). \quad (6)$$

Based on (4) or (6), there are two distinct implementations of the cross-forming regulator.

1) *Explicit Cross-Forming Implementation:* In the first implementation, based on (4), we first aim to design a suitable virtual internal voltage magnitude reference $|\hat{v}_\lambda|$ by enforcing the current magnitude at a prescribed limit. We use an integral regulator aimed at enforcing the current limit to generate this reference. Furthermore, we use the angle reference $\angle \hat{v}$ given by the voltage-forming reference module to finally generate the virtual internal voltage vector reference as $\hat{v}_\lambda = |\hat{v}_\lambda| \angle \hat{v}$. Thus, not only is the angle-forming characteristic preserved, but also the virtual internal voltage magnitude \hat{v}_λ is explicitly made to follow the circuit law as the current limit is enforced.

This is implemented as

$$|\hat{v}_\lambda| = v^* + \frac{\kappa_i}{s} (I_{\text{lim}} - |\hat{i}|), \quad (7a)$$

$$\hat{i} = \frac{1}{z_v} (|\hat{v}_\lambda| \angle \hat{v} - \underline{v}). \quad (7b)$$

The integrator aims to track the given current limit, which is achieved by dynamically reducing the virtual internal voltage magnitude whenever the current reference exceeds the limit. In other words, the current limiting is accomplished by dropping the voltage level without altering the original angle reference. In a current-saturated steady state, the current settles at the limit, and the virtual internal voltage magnitude settles at the value determined by the circuit law. In this manner, the voltage magnitude reference provided by (7a) and the voltage angle reference provided by the voltage-forming reference module can be used to form the voltage vector reference. Furthermore, the current reference is generated by considering a virtual admittance $1/z_v$ in (7b). The control diagram is shown in Fig. 6(a). Note that the current limiter is not mandatory since the current limitation is directly addressed by the explicit cross-forming regulator. However, it can still be used to limit fast overcurrent transients.

We note that the explicit cross-forming control allows for alternatives to (7). For instance, one can use more advanced controls, e.g., predictive control, to replace the integral control in (7a). Alternatively, one can directly use the measured current $|\hat{i}|$ as the feedback in (7a), bypass (7b), and then treat the voltage vector reference as the modulation voltage without using a current limiter and a current controller. In doing so, it is possible to tune the regulator in (7a) to be sufficiently fast to suppress overcurrents while preserving good small-signal stability performance [23]. This is analogous to the classical single-loop voltage-magnitude (SLVM) control presented in [23], where, in contrast, a proportional current feedback control is employed to emulate a virtual resistor to perform current limiting.

2) *Implicit Cross-Forming Implementation:* The second implementation is based on (6). By substituting the virtual (unknown) variable \hat{v}_λ/μ in (6) with the given voltage vector reference \hat{v} and a gain κ , we present an implicit cross-forming control as

$$\hat{i} = \frac{1}{z_v} \left(\kappa \hat{v} - \frac{\underline{v}}{\mu} \right), \quad (8)$$

where $\kappa \in \mathbb{R}_{>0}$ is a control gain, and $z_v \in \mathbb{C}$ is an adjustable virtual impedance. Using the implicit cross-forming control in (8), we arrive at the following dependence of the virtual internal voltage in the desired circuit,

$$\hat{v}_\lambda = \kappa \mu \hat{v} = z_v \hat{i} + \underline{v}, \quad \lambda = \kappa \mu, \quad (9)$$

which suggests that the internal voltage \hat{v}_λ preserves the same angle as the voltage reference \hat{v} , fulfilling the angle-matching aim, i.e., $\angle \hat{v}_\lambda = \angle \hat{v}$. Furthermore, since the magnitude of the virtual internal voltage is governed by the DoS μ indirectly, it is implicitly made to follow the circuit law.

The control diagram is shown in Fig. 6(b). The proportional-like feedback control in (8) subsumes a classical virtual admittance voltage control as given in (27), with the addition of

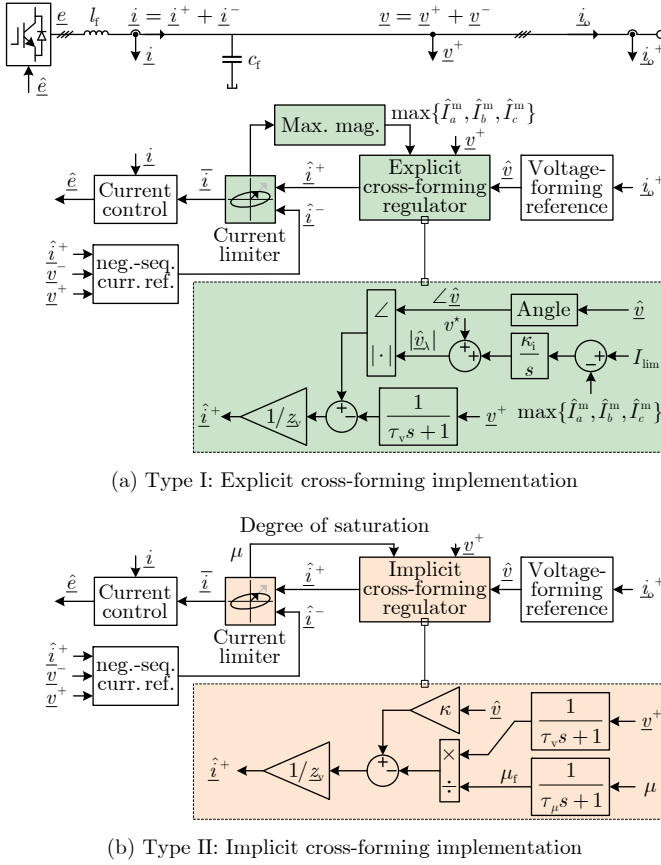


Fig. 6. Proposed cross-forming implementations that maintain voltage-angle-forming and current-magnitude-forming characteristics under current saturation during grid faults. Both implementations are backward compatible with the classical virtual admittance control, facilitating control mode transitions.

the control gain κ and the auxiliary factor $1/\mu$ scaling up the voltage feedback. The feedback DoS signal μ can be easily extracted from the current limiter. A low-pass filter is added to the feedback of μ to make the cross-forming regulating response slower than the current control, and to avoid the appearance of an algebraic loop associated with μ . Moreover, a low-pass filter (for implementation in dq coordinates) or a band-pass filter (for implementation in $\alpha\beta$ coordinates) is added to the voltage feedback to enhance the small-signal stability of the virtual admittance control [35], particularly in the case of a large X/R ratio in \hat{z}_v .

We note that the implicit cross-forming control also allows for alternatives to (8). For example, we show one alternative,

$$\hat{i} = \kappa \frac{\hat{v}}{v/\hat{i} + \hat{z}_v}, \quad (10)$$

which is approximately equivalent to (8). However, it is not compatible with the virtual admittance control structure.

3) *Extensions to Unbalanced Conditions:* Both implementations of cross-forming controls apply to not only balanced conditions but also unbalanced conditions. Particularly, regarding asymmetrical grid faults, the desired equivalent circuit in (3) refers to the positive-sequence circuit. Therefore, all the variables involved in the above design refer to corresponding positive-sequence components. Specifically, concerning asym-

metrical grid faults, the explicit cross-forming regulator in (7) extends to

$$|\hat{v}_\lambda| = v^* + \frac{\kappa_i}{s} (I_{\lim} - \max\{\hat{I}_a^m, \hat{I}_b^m, \hat{I}_c^m\}), \quad (11a)$$

$$\hat{i}^+ = \frac{1}{\hat{z}_v} (|\hat{v}_\lambda| \angle \hat{v} - v^+), \quad (11b)$$

with the phase current magnitude references \hat{I}_x^m , $x \in \{a, b, c\}$. See (47) or (49) in Appendix C for how to calculate \hat{I}_x^m with the positive- and negative-sequence current references given in $\alpha\beta$ or dq coordinates, respectively. Moreover, the implicit cross-forming regulator in (8) extends to

$$\hat{i}^+ = \frac{1}{\hat{z}_v} \left(\kappa \hat{v} - \frac{v^+}{\mu} \right), \quad (12)$$

where the DoS feedback variable is extended from (5) to

$$\text{DoS (unbalanced): } \mu \stackrel{(\text{saturated})}{=} \frac{I_{\lim}}{\max\{\hat{I}_a^m, \hat{I}_b^m, \hat{I}_c^m\}}, \quad (13)$$

where the phase current magnitude references can be extracted from the current limiter, see (47) and (49).

Remark 2. Negative Feedback Regulation: In Fig. 6, a feedback control loop is introduced in both cross-forming implementations. The proper operation of the regulators is based on negative feedback of the control loop. Given the voltage reference angle $\angle \hat{v}$ and the current magnitude limit I_{\lim} , there exist two possible operating points when operating the cross-forming control. This is indicated by the two intersection points in Fig. 3(c). We note that the one with a larger voltage magnitude is a stable operating point, while the other is unstable. We show that this is true by considering that a disturbance leads to an increase in $|\hat{i}|$. This would cause μ , as defined in (5), to decrease. We require that our feedback be such that the decrease in μ would lead to a decrease in $|\hat{i}|$. Since $|\hat{i}| = |1/\hat{z}_v| |\kappa \hat{v} - v/\mu|$, this is only possible if the length of the projection of the vector $\kappa \hat{v}$ onto the direction of v/μ is greater than $|v/\mu|$. Likewise, the negative feedback of $|\hat{i}|$ in (7) requires that the projection of the vector $|\hat{v}_\lambda| \angle \hat{v}$ onto the direction of \hat{v} is larger than $|v|$ so that $|\hat{i}| = |1/\hat{z}_v| |\hat{v}_\lambda| \angle \hat{v} - v|$ decreases when $|\hat{v}_\lambda|$ in (7b) decreases due to a disturbance leading to an increase in $|\hat{i}|$. Therefore, the operating point with a longer virtual internal voltage vector would satisfy the negative feedback requirement. Moreover, corresponding to this operating point, the resulting output current vector lags the internal voltage vector, implying reactive current injection and therefore satisfying grid code requirements.

Remark 3. Recovery to the Normal Control: After fault recovery, when the current exits saturation, the control module in between the voltage-forming reference module and the current limiter is typically a standard virtual admittance control [36]. Since both cross-forming controls subsume a virtual admittance control, recovering the normal voltage-forming control from the cross-forming control is manageable. The reduction of the explicit cross-forming control to the virtual admittance control is obtained by disabling the integrator in (7a) and replacing v^* with the original reference $|\hat{v}|$. Moreover, setting $\kappa = 1$ the implicit cross-forming regulator in (8) simplifies to the virtual admittance control, as $\hat{i} = \hat{i}$ implies $\mu = 1$.

Remark 4. Comparison and Selection Between Both Implementations: Both cross-forming implementations show similarly superior dynamic performance (validated later), provided that their parameters are well-tuned. In terms of their implementations, the implicit cross-forming regulator is closer to the original virtual admittance control with $\mu = 1$ by default. Moreover, tuning the implicit cross-forming regulator is simpler, where $\kappa = 1$ is a straightforward choice. Finally, the implicit implementation can also act faster since no additional control dynamics are introduced, apart from the low-pass filter. Roughly speaking, the implicit cross-forming control may be the first choice between both implementations.

C. Enhanced Voltage-Forming References

The voltage-forming reference is a crucial module of the cross-forming control, as seen in Fig. 5. In this section, we enhance the voltage-forming reference module to improve the transient stability of the cross-forming control. We show in Section IV that the proposed enhancement renders the closed-loop system conform to the canonical form of the standard voltage-forming system. Thus, we can extend existing transient stability results in the literature to current-saturated conditions.

Three types of voltage-forming controls have been reviewed in Appendix A: 1) single-input single-output linear controls, e.g., droop control and VSM, 2) multivariable nonlinear controls, e.g., complex droop control and dVOC, and 3) dual-port control. The enhancement of these voltage-forming controls is based on the coordinates they employ. The most typical coordinates are the \hat{v} and $\hat{\theta}$ polar coordinates, and the other typical ones are \hat{v}_α and \hat{v}_β rectangular coordinates, as used by the recently prevalent dVOC. We show different enhancements concerning different coordinates of voltage-forming controls.

Enhanced Voltage Forming Reference in Polar Coordinates: For a voltage-forming control in polar coordinates, we enhance it by improving the active power feedback as

$$p = \text{Re}\{\hat{v} \text{conj}(\hat{i}_o^+)\}, \quad (14)$$

where $\hat{v} = \hat{v} \angle \hat{\theta}$ is the voltage vector reference, $\text{conj}(\cdot)$ represents a conjugate operation, and \hat{i}_o^+ is the measured positive-sequence current. In the power computation in (14), we use the voltage reference \hat{v} instead of the measured terminal voltage \hat{v}^+ . This power feedback enhancement is depicted in Fig. 7(a). Additionally, since the terminal voltage magnitude is not independently controlled during current saturation (cf. Proposition 1), it is preferable to disable the original voltage magnitude droop control. Instead, we can directly specify a fixed voltage magnitude reference [26], which improves transient stability. This enhancement enables us to arrive at a standard form of power flow feedback and recover an equivalent normal form (shown later in Section IV-A).

Enhanced Voltage Forming Reference in Rectangular Coordinates: For a voltage-forming control in $\alpha\beta$ coordinates, e.g., dVOC, we enhance it by improving the current feedback as

$$\hat{i}_\lambda^+ = \frac{\hat{i}_o^+}{\lambda}, \quad (15)$$

where λ takes $|\hat{v}_\lambda|/|\hat{v}|$ for the explicit cross-forming control, with $|\hat{v}_\lambda|$ given from (7a), while λ takes $\kappa\mu_f$ as given from (9)

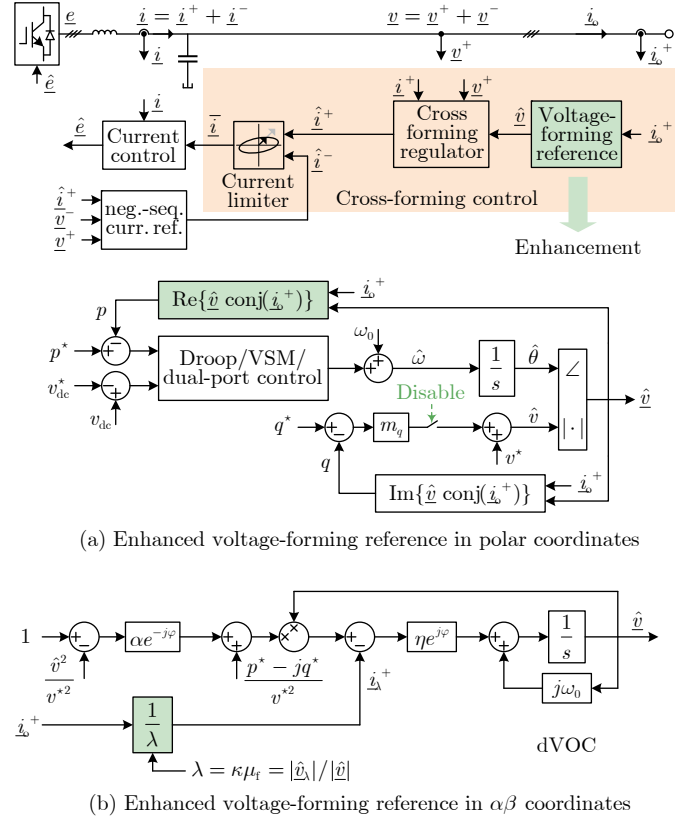


Fig. 7. Enhanced voltage-forming reference module embedded in the cross-forming control, where droop control, VSM, and AC-DC dual-port control in polar coordinates and dVOC in $\alpha\beta$ coordinates are involved.

for the implicit cross-forming control. The enhanced dVOC is depicted in Fig. 7(b). In this manner, we can correspondingly recover an equivalent normal form of dVOC (shown later in Section IV-B).

When the current exits saturation after grid fault recovery, we can easily recover the enhanced control in Fig. 7(a) to the normal voltage-forming reference by restarting the voltage droop control, and likewise we can restore the normal dVOC from the enhanced dVOC in Fig. 7(b) by resetting $\lambda = 1$.

D. Benchmarking Against Existing Strategies

We present a comparative analysis of the proposed cross-forming control versus typical existing strategies regarding the current limiting of grid-forming inverters. Table II summarizes the key features and performance metrics of these strategies, categorizing them into voltage-forming-based, current-forming-based, and cross-forming-based strategies.

The current-limiting strategies previously investigated for grid-forming inverters encompass two main types: voltage-forming-based and current-forming-based strategies. As reviewed in Appendix C, voltage-forming-based strategies include two types: Type-A, characterized by adaptive virtual impedance mechanisms (also known as threshold virtual impedance) [8], [9], and Type-B, characterized by a current limiter cascaded with a virtual admittance [10]–[14]. Conversely, current-forming strategies typically specify current

TABLE II
BENCHMARKING OF THE PROPOSED CROSS-FORMING STRATEGIES AGAINST EXISTING CURRENT-LIMITING STRATEGIES.

	Voltage-forming strategies	Current-forming strategies	Cross-forming strategies
Current limiting strategies	<ul style="list-style-type: none"> Type-A: Adaptive virtual impedance [8], [9] Type-B: Current limiter with virtual admittance [10]–[14] 	Current reference direct specification [15]–[18] or in a drooped way [20], [21]	<ul style="list-style-type: none"> Type-I: Explicit cross-forming Type-II: Implicit cross-forming
Forming behaviors	<ul style="list-style-type: none"> Internal voltage forming Current magnitude constrained 	<ul style="list-style-type: none"> Current forming Voltage following (undesired) 	<ul style="list-style-type: none"> Voltage angle forming Current magnitude forming
Control switching	No switching needed	Yes and incompatible	Yes but compatible
Current-limiting speed	<ul style="list-style-type: none"> Slow if using Type-A Fast if using Type-B 	Fast	Fast
Overcurrent utilization	<ul style="list-style-type: none"> No, for Type-A, limited within $[I_{th}, I_{lim}]$ Yes, for Type-B, limited at I_{lim} 	Yes, limited at I_{lim}	Yes, limited at I_{lim}
FRT i_Q provision	i_Q naturally provided, with high priority by reducing p^*	<ul style="list-style-type: none"> Adjust i_Q^* if using PLL, but slow Reduce p^* if using angle-forming [15], but i_Q provision may be slow 	i_Q naturally provided, with high priority by reducing p^*
Phase jump i_P provision	i_P naturally provided	i_P can be favorable or adverse due to behaving as a current source	i_P naturally provided
Tuning complexity	<ul style="list-style-type: none"> Complicated if using Type-A Simple if using Type-B 	Simple for current limiting, but complicated for FRT services	Simple
Resulting impedance	Current-dependent for both Type-A and -B	NA	Constant
Transient stability enhancements	Numerous strategies available, e.g., <ul style="list-style-type: none"> Virtual-power feedback [11] Alternating virtual inertia [37] Mode-adaptive control [38] Power setpoint adjusting [39] Transient active power control [40] 	<ul style="list-style-type: none"> Q-axis voltage feedback [15] Current reference angle adjusting [16]–[18], but may conflict with FRT services requirements 	<ul style="list-style-type: none"> Enhanced voltage-forming references
Transient stability analysis	Difficult since the resulting virtual impedance is current-dependent	Relatively difficult due to involving control architecture switching	Equivalent normal forms allow extending existing methods

references directly in the current-forming control setup [16]–[18]. The developed cross-forming strategies can be implemented in an explicit (Type I) and in an implicit (Type II) manner. The merits of both the voltage-forming and current-forming strategies are preserved as the proposed cross-forming strategy enables forming characteristics for voltage angle and current magnitude.

A critical aspect of the difference among the strategies is the switching between control architectures. Voltage-forming-based strategies do not necessitate control switching, while current-forming-based strategies typically require us to switch the entire control architecture. In contrast, cross-forming-based strategies feature backward compatibility of control architecture since a typical virtual admittance control is subsumed. Thus, we can avoid a complete switching between control architectures. Furthermore, we evaluate the speed of current limiting, indicating that Type-A voltage-forming-based strategies demonstrate a relatively slow response, since a virtual impedance control is typically located outside the voltage control loop. The other strategies exhibit fast rapidity because of the use of a current limiter. Moreover, Type-A voltage-forming-based strategies cannot guarantee full overcurrent utilization, while the other ones fully utilize the overcurrent limit. Furthermore, we investigate FRT services (fault reactive current i_Q and phase jump active current i_P provision), highlighting the differing responses between strategies. In particular, cross-forming-based strategies offer natural i_Q and i_P provisions within the current limit, similar to voltage-forming-based strategies. In contrast, current-forming-based strategies may not be able to provide a natural response as fast as a voltage source to fulfill the requirements of FRT services. Moreover, cross-forming strategies feature simple parameter tuning simi-

lar to Type-B voltage-forming strategies. In contrast, the tuning of Type-A voltage-forming strategies is complicated since it involves the consideration of the worst case [8], where it is not straightforward to take a negative-sequence current into account in the case of asymmetrical grid faults. Finally, we discuss the resulting equivalent circuits and transient stability, emphasizing the challenges posed by a current-dependent virtual impedance in voltage-forming-based strategies and control switching in current-forming-based strategies. In contrast, cross-forming-based strategies result in a constant equivalent impedance, demonstrating compatibility with existing analysis methods, as presented in the next section.

IV. EQUIVALENT NORMAL FORMS AND TRANSIENT STABILITY ANALYSIS EXTENSION

The transient stability of voltage-forming systems is rooted in the closed-loop relationship between the voltage-forming control and the grid network. Numerous transient stability results have been reported in the literature, but these results are primarily concentrated on the normal form of voltage-forming systems, where the current is assumed to be unsaturated. In this work, we extend the existing stability analysis methods and results to the case of current saturation. This becomes feasible since the cross-forming control renders a desired equivalent circuit as shown in Fig. 5. In this section, we first consider the cross-forming control with the enhanced voltage-forming reference to recover an equivalent system that conforms to the normal/canonical system form. Then, we extend existing stability results concerning the normal form to the system under current saturation.

A. Equivalent Normal Form in Polar Coordinates

Consider the cross-forming control architecture that embeds an enhanced voltage-forming reference in polar coordinates. The equivalent system shown in Fig. 8(a) depicts a closed-loop connection between the enhanced voltage-forming reference and the equivalent circuit given earlier in Fig. 5. The equivalent circuit incorporates a cross-forming source that results from the cross-forming control. Fig. 8(a) also shows the normal form of the system in the case of current unsaturation. The transient stability of the normal-form system has been widely investigated with the angle-forming control in closed loop with the so-called power-angle relationship, where the voltage magnitude is typically assumed to be constant. We show in the following that the equivalent system maintains the same closed-loop nonlinear synchronization dynamics (i.e., transient stability characteristics) as the normal-form system. To show this, we simply need to show that the active power feedback (i.e., the power-angle relationship) is equivalent, given that the angle-forming control dynamics remain consistent.

Consider a typical assumption that the grid network is dominantly inductive, i.e., $z_v = jx_v$. The virtual internal voltage is denoted by \hat{v}_λ as in the equivalent circuit in Fig. 5. We consider that the inverter is connected to a Thevenin equivalent grid with voltage $\underline{v}_g := v_g \angle \theta_g$ and grid impedance $z_g := jx_g$. The power feedback of the equivalent system, as given in (14), is expanded as

$$\begin{aligned}
 p &= \text{Re}\{\hat{v} \text{conj}(\hat{i}_o^+)\} \\
 &= \text{Re}\left\{\hat{v} \angle \hat{\theta} \text{conj}\left(\frac{|\hat{v}_\lambda| \angle \hat{\theta} - v_g \angle \theta_g}{jx_v + jx_g}\right)\right\} \\
 &= \text{Re}\left\{j \frac{\hat{v} |\hat{v}_\lambda| - \hat{v} v_g \angle (\hat{\theta} - \theta_g)}{x_v + x_g}\right\} \\
 &= \frac{\hat{v} v_g}{x_v + x_g} \sin(\hat{\theta} - \theta_g),
 \end{aligned} \tag{16}$$

where it is seen that the power-angle relationship conforms to the normal sine function form. Hence, the equivalent system shares the same transient stability characteristics as the normal-form system. If we further consider $\hat{v} = v^*$, the power-angle relationship will be independent of the voltage reference dynamics. We note that the result can be extended to a more general case where the network is not necessarily inductive but has a uniform X/R ratio. Moreover, the result in (16) may be extended to multi-inverter networks, in which the coefficients of the sine terms in the active power flow equation will rely on the virtual internal voltage magnitude of the current-saturated nodes and the terminal voltage magnitude of the current-unsaturated nodes.

B. Equivalent Normal Form in Rectangular Coordinates

Consider the cross-forming control architecture embedding an enhanced voltage-forming control in rectangular coordinates (specifically, dVOC). The equivalent system is shown in Fig. 8(b), which likewise, depicts a closed-loop connection between the enhanced dVOC and an equivalent circuit. The normal form of the system is also shown in Fig. 8(b). The

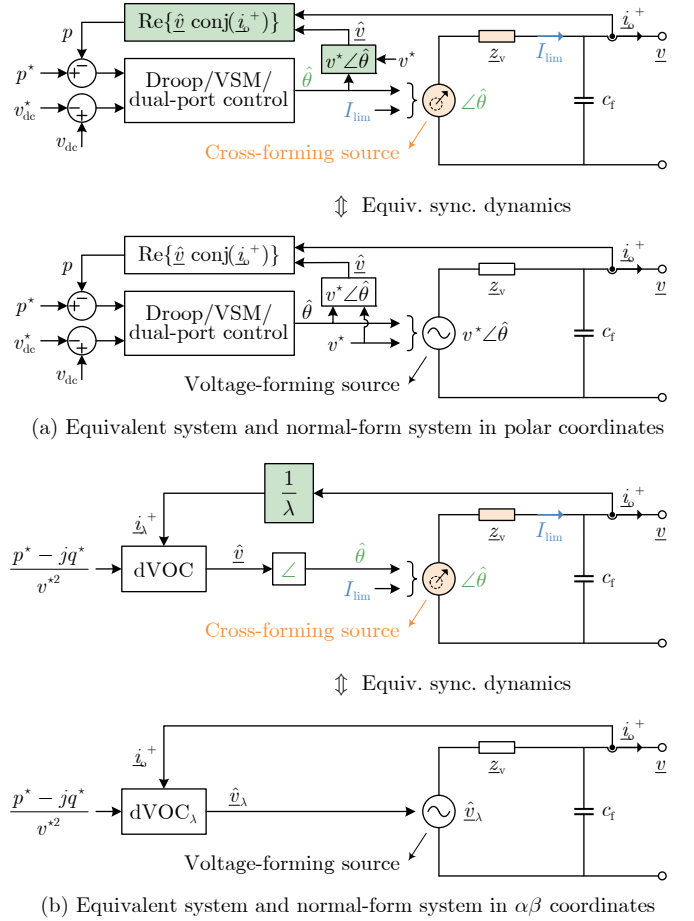


Fig. 8. The equivalent system, resulting from the cross-forming regulator and the enhanced voltage-forming reference, maintains equivalent transient synchronization dynamics to the normal-form system, allowing us to extend existing transient stability results to current-saturated conditions.

transient stability of the normal form of dVOC has been explored based on the dVOC dynamics in closed loop with the network voltage-current relationship, where the dynamics in both rectangular coordinates are included. We indicate, in the following, that the equivalent system is equivalent to the normal-form system in terms of the closed-loop nonlinear synchronization dynamics.

Consider the enhanced dVOC in Fig. 7(b),

$$\dot{\hat{v}} = j\omega_0 \hat{v} + \eta e^{j\varphi} \left(\frac{p^* - jq^*}{v^{*2}} \hat{v} - \frac{\hat{i}_o^+}{\lambda} \right) + \eta \alpha \frac{v^{*2} - \hat{v}^2}{v^{*2}} \hat{v}, \tag{17}$$

which further gives rise to

$$\dot{\hat{v}_\lambda} = j\omega_0 \hat{v}_\lambda + \eta e^{j\varphi} \left(\frac{p^* - jq^*}{v^{*2}} \hat{v}_\lambda - \hat{i}_o^+ \right) + \eta \alpha \frac{v_\lambda^{*2} - \hat{v}_\lambda^2}{v_\lambda^{*2}} \hat{v}_\lambda, \tag{18}$$

where $\hat{v}_\lambda = \lambda \hat{v}$ and $v_\lambda^* := \lambda v^*$, and the dynamics of λ is ignored for ease of analysis. This indicates that (18), shaped by the enhanced dVOC, describes the virtual internal voltage dynamics¹. It can be seen that the dynamics in (18) conform

¹The derivation of the equivalent internal voltage dynamics in (18) is only aimed for us to analyze stability; it does not imply that the internal voltage \hat{v}_λ can be imposed independently, since the internal voltage magnitude $\lambda|\hat{v}|$ inherently follows the circuit law, cf. Prop. 1.

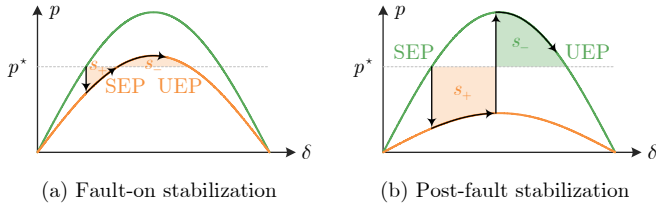


Fig. 9. Transient stability of grid-forming inverters during (a) the fault-on period and (b) the post-fault period. The fault-on power-angle curve, as given in (16), has the same shape as the normal one regardless of whether the current is saturated or not.

to the normal form of dVOC. Thus, the equivalent system shares the same transient stability characteristics (mainly in synchronization) as the normal-form system.

C. Transient Stability Results Extended to Current Saturation

Based on the equivalent normal form obtained earlier, we now extend typical existing transient stability results to the case of current saturation. We focus on the extension concerning a single-inverter infinite-bus system for ease of understanding. We refer to [41]–[44] for more comprehensive results for multi-inverter systems.

As noted earlier, the transient stability of a voltage-forming control in polar coordinates is analyzed with the so-called power-angle relationship [45]. Fig. 9 illustrates typical power-angle curves of a voltage-forming source connected to a dominantly inductive grid with a normal grid voltage, a slight voltage dip in Fig. 9(a), and a severe voltage dip in Fig. 9(b). It can be seen that the three power curves are with the same shape. If there exist stable equilibrium points (SEPs), i.e., p^* intersects with the fault-on power-angle curve, the system may achieve (fault-on) transient stability during the grid voltage dip. More specifically, for a dominantly first-order angle-forming control (e.g., droop control), the transient stability can be maintained provided that the equilibrium point is present. For a dominantly second-order angle-forming control (e.g., VSM and dual-port control), the transient stability during the grid voltage dip is determined by the difference between the accelerating area s_+ and the decelerating area s_- . If there are no equilibrium points during the voltage dip, the system cannot achieve synchronization but possibly achieve (post-fault) synchronization after grid voltage recovery. Likewise, the transient stability is determined by the sufficiency of the decelerating area s_- to counteract the accelerating area s_+ . The equal-area criterion, as a conservative yet simple stability criterion inherited from conventional power systems, has been widely used to analyze and improve the transient stability of grid-forming inverters. Alternatively, one may resort to the energy function method for transient stability assessment, for example, a typical energy function of VSMs is given as [46]

$$V(\omega, \delta) = \frac{1}{2} T_J \omega^2 - p_{\max} (\cos \delta - \cos \delta_0) - p^* (\delta - \delta_0), \quad (19)$$

with the inertia time constant T_J , the post-fault power transfer limit p_{\max} , and the post-fault stable equilibrium point δ_0 . The energy function and the information on the post-fault unstable equilibrium point (UEP) can be used to approximate the

stability region and identify the critical clearance time of the grid fault [47]. Additionally, in actual applications, e.g., grid-forming inverters connect renewable energy such as wind or photovoltaic to the grid, the active power setpoint p^* of the inverter as well as the active power from the primary energy source side should be reduced during grid voltage dips to respect the power transfer limit of the transmission line and to prioritize FRT services such as fault reactive current provision.

The transient stability of dVOC is typically analyzed in both rectangular α and β coordinates [48]. Without relying on the power-angle relationship, the equal-area criterion, or the energy function method, a standard Lyapunov stability analysis has been presented in our earlier work. For the recovered equivalent system in (18) connected to an infinite grid, a sufficient condition for transient stability is recalled from [48],

$$\operatorname{Re}\left\{e^{j\varphi} \frac{p^* - jq^*}{v^{*2}}\right\} + \alpha < \frac{\alpha}{2} \frac{\hat{v}_{\lambda s}^2}{v^{*2}} + \operatorname{Re}\{e^{j\varphi} \underline{y}\}, \quad (20)$$

where $\hat{v}_{\lambda s}^2$ is the steady-state magnitude of the internal voltage $\underline{\hat{v}}_{\lambda}$, and $\underline{y} = 1/(\underline{z}_v + \underline{z}_g)$ denotes the admittance of the lumped impedance seen from the virtual internal voltage to the infinite bus. This stability condition provides quantitative insights for parameter tuning, system operation, etc. See our results in [49] for more extensions regarding multi-inverter systems.

V. SIMULATION AND EXPERIMENTAL VALIDATIONS

We present case studies to validate the performance of the proposed cross-forming control. In Case Study I, we validate the performance of both cross-forming implementations (explicit and implicit) under a symmetrical grid fault. In Case Study II, we show the result of the recommended implicit cross-forming control under an asymmetrical grid fault, where four different negative-sequence control modes are validated. In Case Study III, the performance of the cross-forming control is validated in multi-inverter grid-connected and islanded systems. In Case Study IV, we compare the performance against three typical strategies. Finally, the experimental validations are presented. Our validations consider VSM as a typical representative of grid-forming reference in polar coordinates. The validation of grid-forming in rectangular coordinates (e.g., dVOC) can follow the same steps, which have been reported in our earlier work [49].

The system models in the simulation are depicted in Fig. 10, where a single-inverter system, a multi-inverter grid-connected system, and the IEEE 9-bus system with three inverters are included. The grid faults are simulated on the high-voltage network through a grounding resistor r_f . Table III(a) summarizes main system parameters and controller parameters. The grid-forming inverters are configured with cascaded control loops, as shown in Fig 19, where the inner control loops are implemented in the dq rotational reference frame, with the only exception that the current control for unbalanced grid conditions is implemented in the $\alpha\beta$ stationary reference frame to avoid the impact of delays in the extraction of sequence components, ensuring a sufficiently high current control bandwidth. Since the voltage controller is arranged as a static virtual admittance element, in contrast to conventional PI/PR

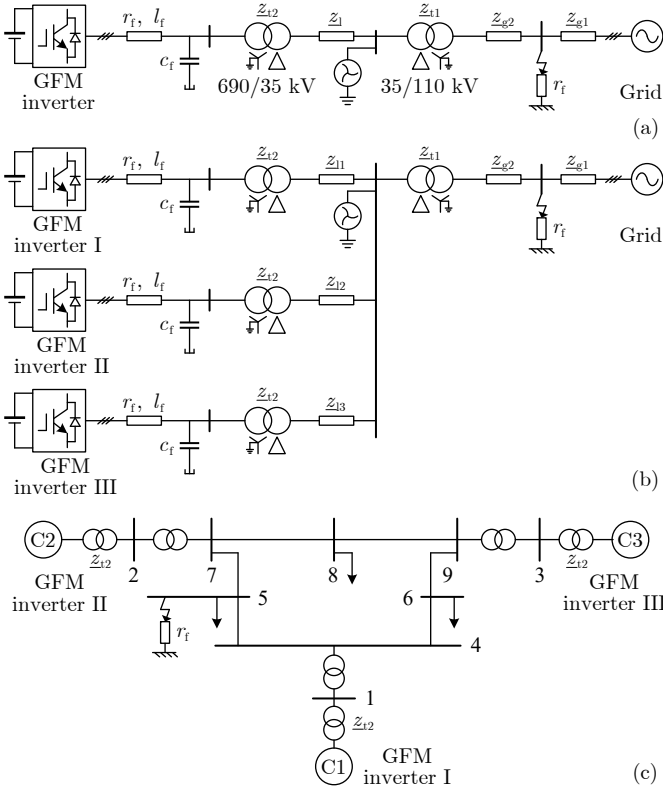


Fig. 10. Illustration of the system models in Case Studies. (a) A single-inverter system in Case Studies I, II, and IV. (b) A multi-inverter system in Case Study IIIa. (c) IEEE 9-bus system in Case Study IIIb.

dynamic regulators, the difficulty of managing the interaction of the inner voltage and current control loops is significantly reduced. As a result, the controller parameter tuning becomes simple, allowing a large range of parameter value choices.

A. Case Study I: Symmetrical Grid Faults

The result of Case Study I is shown in Fig. 11. A symmetrical short-circuit fault occurs at 3 s in between z_{g1} and z_{g2} in the system of Fig. 11(a). The inverter without using any current-limiting strategies immediately suffers from overcurrent, as can be seen in Fig. 11(a). In Fig. 11(b) and 11(c), in contrast, both the explicit and implicit cross-forming controls successfully limit the inverter current at the prescribed limit 1.1 pu rapidly due to their inherent current-magnitude-forming capability, and both perform very similarly. Since the current is saturated, the power injection is consequently reduced compared to the unlimited scenario, indicating the actual capability of the inverter to provide FRT services under current limits. It can be seen that the reactive power injection increase is fast after the grid fault happens, such that the reactive power/current response can satisfy the fault current specifications in grid codes. This is attributed to the angle-forming functionality of the cross-forming control. In other words, the virtual internal voltage vector remains the same angle as the pre-fault at the fault occurrence moment (and then slowly exhibits an inertial response). The reactive current component in the fault current naturally increases at the fault

TABLE III
PARAMETERS IN SIMULATION STUDIES AND EXPERIMENTS

Symbol	Description	Value
(a) Parameters in simulation Case Studies I–IV		
S_N	Nominal capacity	I, II, IV: 200 MVA IIIa: 200/3 MVA for each IIIb: 247.5, 192, 128 MVA
ω_0	Fundamental frequency	100 π rad/s
z_{g1}	Grid impedance	0.01 + j 0.1 pu
z_{g2}	Grid impedance	0.003 + j 0.03 pu
z_1	Line impedance	0.01 + j 0.05 pu
z_{11}	Line impedance	0.01 + j 0.05 pu
z_{12}	Line impedance	0.02 + j 0.10 pu
z_{13}	Line impedance	0.03 + j 0.15 pu
z_{t1}	Transformer impedance	0.16/30 + j 0.16 pu
z_{t2}	Transformer impedance	0.06/30 + j 0.06 pu
r_f	Fault grounding resistance	1.0 Ω
l_f	Filter inductance	0.05 pu
r_f	Filter inductance	0.05/10 pu
c_f	Filter inductance	0.05 pu
p^*	Active power setpoint	I, II: 0.2 pu III: 0.5, 0.7, 0.9, pu IV: 0.35 pu
q^*	Reactive power setpoint	I, II: 0.0 pu III: 0.5, 0.3, 0.1 pu IV: 0.0 pu
v^*	Voltage setpoint	I, II, IIIa, IV: 1.0 pu IIIb: 1.1 pu
T_J	Inertia time constant	5 s
D	Damping coefficient	25
m_q	Reactive power droop gain	0.2
z_v	Virtual impedance	I, II, IIIa, IV: j 0.2 pu IIIb: $0.2e^{j5\pi/12}$ pu
τ_v	LPF time const. in \underline{v} feedback	0.01 s
τ_μ	LPF time const. in $\underline{\mu}$ feedback	0.02 s
κ	Cross-forming feedforward gain	1
κ_i	Cross-forming integral gain	50
κ_{vi}	Feedback gain in adaptive VI	0.91
σ_{vi}	X/R ratio in adaptive VI	10
k^-	K -factor in neg.-seq mode IV	6
I_{lim}	Current limit	1.1 pu
(b) Parameters in experiments		
U_{rms}	Line-to-line voltage level	200 V
S_N	Nominal capacity	1 kVA
ω_0	Fundamental frequency	100 π rad/s
L_f	Filter inductance	1.5 mH (0.012 pu)
R_f	Filter inductance	1.0 Ω (0.025 pu)
C_f	Filter inductance	3.5 μ F (0.044 pu)
G_{load}	Resistor load conductance	0.124 pu
z_g	Grid impedance (emulated)	j 0.2 pu
p^*	Active power setpoint	0.1 pu
q^*	Reactive power setpoint	0.0 pu
v^*	Voltage setpoint	1.1 pu
z_v	Virtual impedance	j 0.1, j 0.6 pu
f_{sw}	Switching frequency	32 kHz
f_s	Sampling and control frequency	8 kHz

moment, as explained in Fig. 4(c). To provide more reactive power/current during the fault, one can reduce the power angle by lowering the active power setpoint. It can also be observed from Fig. 11 that the phase angle gradually goes down before the fault clearance, which is because the (Thevenin) equivalent grid voltage undergoes a phase jump backward at the fault moment. If the fault duration is long enough and the power setpoint is not too large, the inverter will synchronize with the faulty grid within the fault stage and settle down to a steady state. The inertial response and the synchronization behavior are due to the preservation of the angle-forming capability in

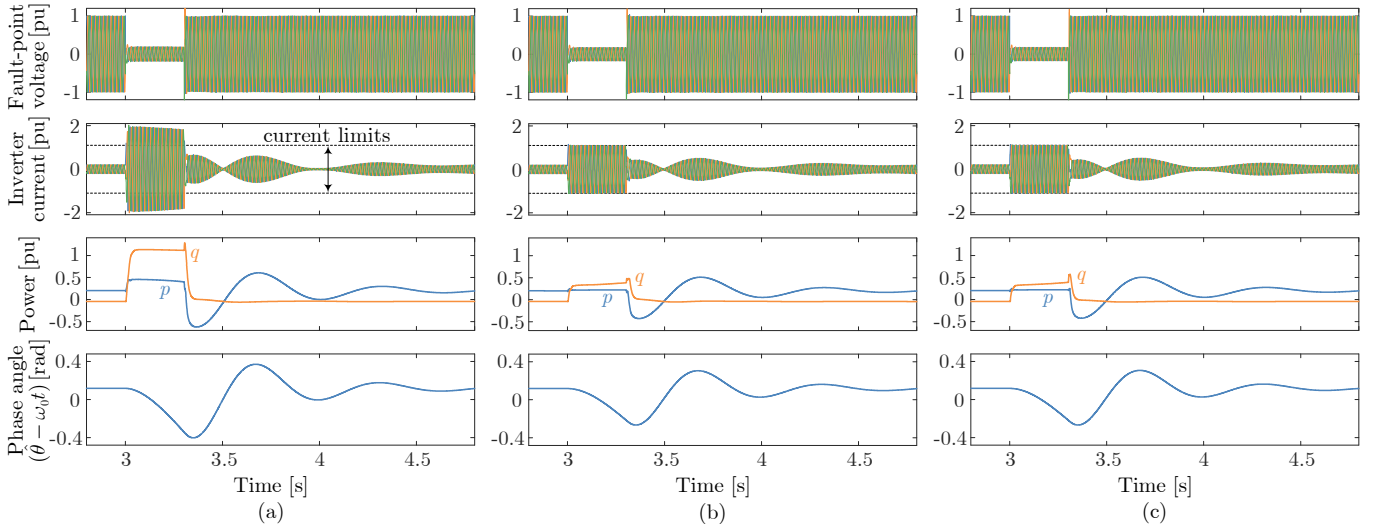


Fig. 11. Result of Case Study I under a symmetrical grid fault: (a) Without using any current-limiting strategies; (b) With the explicit cross-forming control under the grid fault. (c) With the implicit cross-forming control under the grid fault.

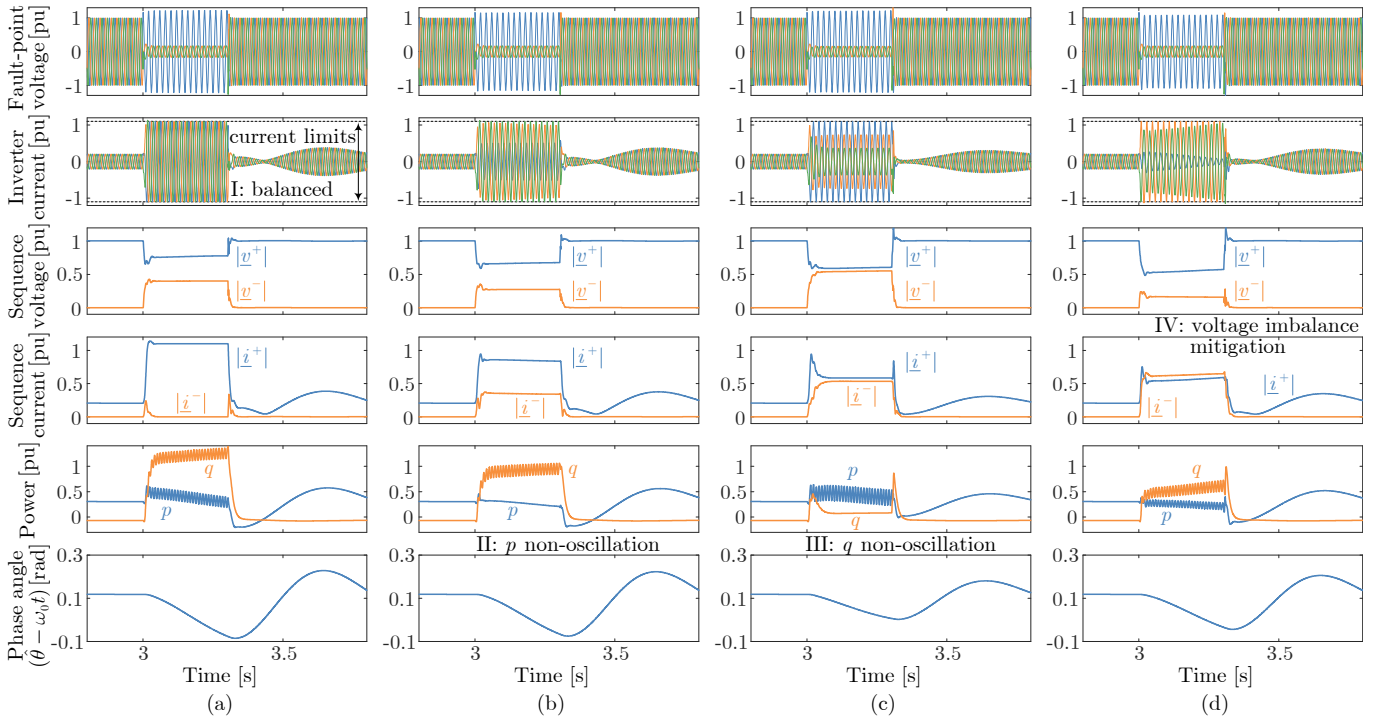


Fig. 12. Result of Case Study II under an asymmetrical grid fault: (a) Mode I – Balanced current control; (b) Mode II – Active power oscillation suppression; (c) Mode III – Reactive power oscillation suppression; (d) Mode IV – Negative-sequence voltage mitigation.

the cross-forming control.

The fault is cleared at 3.3 s, and the feedback of μ in the voltage control is disabled when the fault clearance is detected. This ensures that the normal control is restored. If the feedback remains enabled, μ may converge to zero undesirably since the negative feedback in the cross-forming control may not survive during grid fault recovery. After restoring the normal control, the active power and the phase angle undergo an inertial response and finally stabilize at the pre-fault steady state. To obtain transient stability guarantees for either the fault-on stage

or the post-fault stage, one can apply the extended method in Section IV-C to deal with the fault-on current-saturated stage. This is feasible due to benefiting from the resulting constant equivalent impedance in the equivalent circuit and the resulting equivalent normal form based on the improved power feedback in the enhanced VSM reference.

B. Case Study II: Asymmetrical Grid Faults

The result of Case Study II is shown in Fig. 12. An asymmetrical short-circuit fault (double line-to-ground fault) occurs

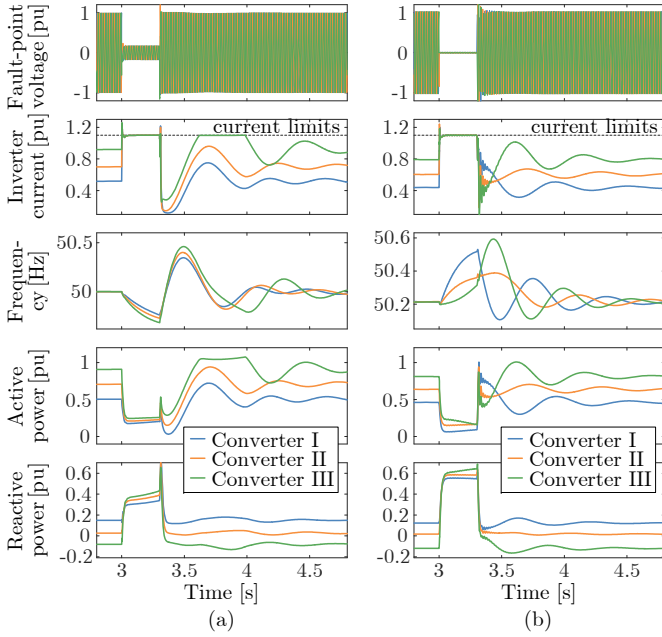


Fig. 13. Result of Case Study III: (a) Three-inverter grid-connected system; (b) IEEE 9-bus system with three inverters.

at 3 s. As can be seen from Fig. 12, the fault-point voltage becomes unbalanced during the fault, where the voltages of faulty phases B and C are declined. The simulation results of four control modes regarding negative-sequence components are presented in Fig. 12(a)–(d), respectively, i.e., the control modes reviewed in Appendix B. More specifically, a balanced current mode is adopted in Fig. 12(a), where it is noticed that the inverter current remains balanced. In Fig. 12(b)/(c), an active/reactive power oscillation suppression mode is employed, where it is observed that the active/reactive power is non-oscillatory. A negative-sequence voltage mitigation mode is operated in Fig. 12(d), where the negative-sequence voltage is reduced by intentionally absorbing negative-sequence inductive reactive current via a virtual inductance as in (34), satisfying the negative-sequence service required in grid codes. It is observed, however, that the positive-sequence voltage is reduced as well compared to the result in Fig. 12(a), which is because the positive-sequence reactive current component is compromised and also due to the coupling between the sequence networks similar to a grid-following case [31]. We observe from Fig. 12 that under any negative-sequence control mode, the maximum phase current magnitude is limited at the prescribed value, demonstrating that the cross-forming control is feasible under asymmetrical faults and flexibly applies to multiple negative-sequence control modes.

C. Case Study III: Multi-Inverter Scenarios

The result of Case Study III is shown in Fig. 13, where Case Studies IIIa and IIIb are presented.

1) *Case Study IIIa*: A symmetrical short-circuit fault occurs at 3 s in the grid-connected system in Fig. 10(b). The three inverters have the same power ratings but different power setpoints and different line impedance values to the point of

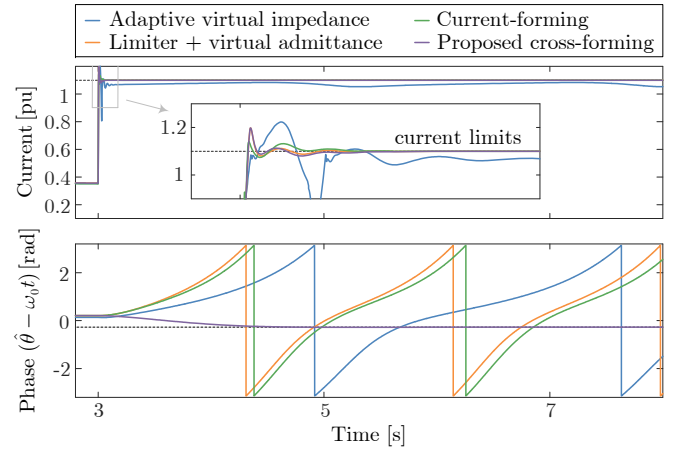


Fig. 14. Result of Case Study IV: Performance comparison of the proposed implicit cross-forming strategy against three typical strategies.

common coupling (PCC), as indicated in Table III(a). The simulation result shows that the inverters successfully ride through the grid fault, their currents remain limited at/within the prescribed value during and after the fault, and reactive power is injected during the fault. Since the three-phase currents are slightly distorted due to transients at the fault occurrence and clearance moments, the 2-norm current magnitude expression $|i_\alpha + ji_\beta|$ cannot precisely represent the phase current peaks. Therefore, even though the transient peak of the 2-norm current magnitude exceeds the limit, the actual phase current magnitudes (∞ -norm) remain within the limit. It is important to note that the active power setpoints are reduced to 0.2 pu during the grid voltage dip, which is to prioritize the reactive power injection and to alleviate the accumulation of active power imbalance during the voltage dip for improving transient stability. The inverters achieve transient stability after grid fault recovery, and the current limit may be touched again (see the green waveform) during the stabilization.

2) *Case Study IIIb*: A symmetrical short-circuit fault occurs at 3 s in the IEEE 9-bus system in Fig. 10(c). The three inverters have different power ratings and different power setpoints, as indicated in Table III(a). The simulation result shows that the inverters successfully ride through the grid fault and their currents remain limited at the prescribed value during the severe grid fault. Likewise, the active power setpoints are reduced during the fault to improve the post-fault transient stability. It is important to note that all the inverters enter the cross-forming operating mode during the grid fault, and as a result, their voltages concurrently follow the current injection based on the circuit law. Since the IEEE 9-bus system contains only constant impedance loads, the system converges to a steady state in the case, similar to the islanded operation of a PLL-based current-forming inverter discussed in [25]. However, if there are voltage-dependent nonlinear loads, the system may require voltage magnitude-forming devices to respond to form the voltage magnitude. This is possible in practice if some grid-forming inverters are far from the fault location and thus do not enter current saturation throughout the fault (i.e., consistently preserving voltage magnitude and angle forming).

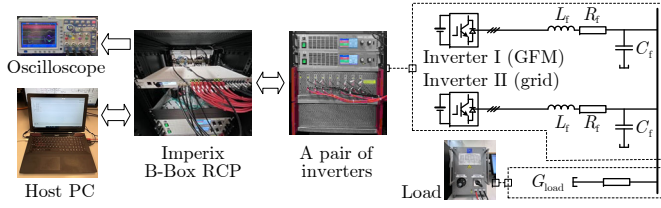


Fig. 15. Experimental setup based on prototype inverters, where inverter II emulates grid voltage, grid impedance, and different grid faults.

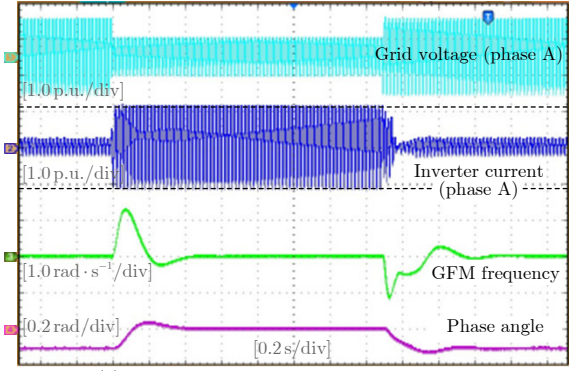
D. Case Study IV: Comparison Against Existing Strategies

The result of Case Study IV is displayed in Fig. 14, where a permanent fault is simulated to investigate the fault-on transient stability. The simulation comparison of the performance between the proposed cross-forming strategy and existing strategies confirms the benchmarking analysis in Section III-D. More specifically, the limiter + virtual admittance strategy, the current-forming strategy, and the proposed cross-forming strategy capably limit the current to the prescribed value rapidly. By comparison, the adaptive virtual impedance is relatively slow, suffering from the limitation of the voltage control bandwidth. Moreover, due to using proportional feedback control, the adaptive virtual impedance cannot fully utilize the over-current limit, i.e., the current is limited under I_{lim} , as observed from Fig. 14. In terms of transient stability, the cross-forming control has a larger stability margin due to the enhancement of the power feedback as in (14). It, therefore, can achieve transient stability even with a higher power setpoint 0.35 pu as given in Table III(a). In contrast, the existing strategies will easily exhibit transient instability behaviors, as observed from the phase angle waveforms in Fig. 14, if we do not apply any transient stability enhancements as reviewed in Table II. It is certainly possible to regain transient stability when using the transient stability enhancements. However, transient stability analysis and guaranteeing still face huge difficulties due to the current-dependent equivalent impedance or the control architecture switching involved in these existing strategies. In contrast, the proposed cross-forming control allows us to readily extend pre-existing transient stability results, a significant advantage that has not yet been established with the existing current-limiting strategies.

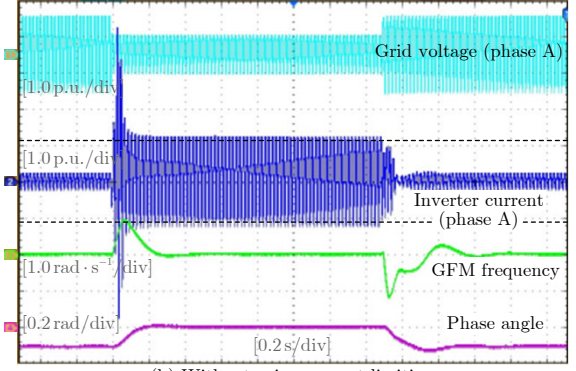
E. Experimental Results

The experimental setup depicted in Fig. 15 is used to additionally validate the performance of the cross-forming control. The setup involves the interconnection of two face-to-face inverters, with one employing a VSM-based voltage-forming reference and the other emulating grid voltage, grid impedance, and different grid faults. Since the DC voltage sources of both inverters are bi-directional, a resistive load G_{load} is connected to the AC bus to consume the power delivered by the inverters. Both inverters are controlled by an Imperix B-Box rapid control prototyping system. The parameters used in the experiments are given in Table III(b).

The experimental result under a symmetrical grid voltage dip is displayed in Fig. 16, where the voltage dips to 0.5 pu



(a) With the proposed current-limiting strategy



(b) Without using current limiting

Fig. 16. Experimental results under a symmetrical grid fault, where the grid voltage dips to 0.5 pu and the phase jumps +15 degrees.

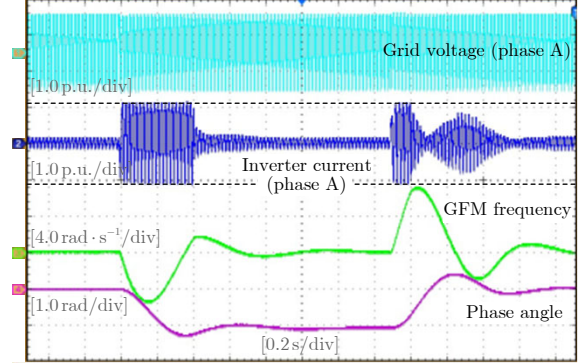


Fig. 17. Experimental results under grid phase jump -60 degrees.

and the phase angle jumps +15 degrees. The current of the grid-forming inverter is limited at the prescribed value when using the proposed cross-forming strategy, as demonstrated in Fig. 16(a). In contrast, when no current limiting is employed, the inverter suffers from an immediate high overcurrent peak and subsequent steady-state overcurrent. Since the active power setpoint is small and the voltage dip lasts long enough for 1.5 s, the inverter synchronizes with the grid (i.e., the other inverter that emulates a grid) and stabilizes.

In Fig. 17, the experimental results under a pure grid phase jump of -60 degrees without any voltage magnitude changes are displayed. We use a larger virtual impedance $z_v = 0.6$ pu to guarantee that there exist feasible operating points under the cross-forming mode consistently during the synchronization.

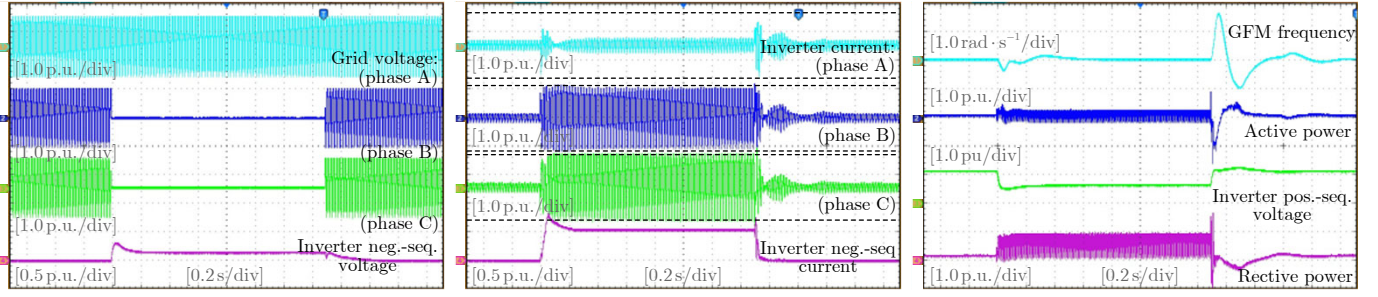


Fig. 18. Experimental results under an asymmetrical grid fault, where phase A voltage remains while phase B and C voltages dip to zero.

In other words, as illustrated in Fig. 4(c), when the power angle between $\angle v$ and $\angle v_g$ suddenly changes to large, a large radius of $|\Delta v_z| = |(z_g + z_v)\dot{z}|$ is required to ensure that the circle of the radius intersects with the angle direction $\angle v$ during the synchronization. Otherwise, the cross-forming control will collapse due to the non-existence of a feasible operating point. From Fig. 17, it can be seen that the overcurrent during the synchronization is properly limited. Throughout the current-limiting process, there are always operating points due to the use of a large virtual impedance. When the synchronization is almost achieved, the overcurrent state exists, and the inverter returns to the original steady state.

Fig. 18 shows the experimental results under an asymmetrical grid voltage dip, where phase A voltage remains while phase B and C voltages dip to zero, emulating a bolted double line-to-ground fault. During the asymmetrical fault, phase C current stays at the limit, phase B current stays close to the limit, and phase A current remains small. The negative-sequence voltage at the inverter terminal is small since the negative-sequence voltage mitigation mode is used. Similar to the result under the symmetrical fault, synchronization is achieved during the fault stage. The performance under the other negative-sequence control modes has also been experimentally validated, which is similar to the simulation results shown earlier.

VI. CONCLUSION

We present the concept of cross-forming for grid-forming inverter control, particularly for operating against grid faults (including symmetrical and asymmetrical faults). The cross-forming concept integrates voltage-angle-forming and current-magnitude-forming characteristics, inherently satisfying grid-forming objectives/specifications under grid faults, including angle-/frequency-forming synchronization (or stability), FRT services provision, fault current limiting, etc. The concept has inspired the development of two feasible control strategies to enable cross-forming operations. Leveraging the resulting equivalent circuit featuring a constant virtual impedance, we establish an equivalent normal form of the system and extend previously established transient stability results from unsaturated to saturated conditions. The extension makes transient stability analysis, assessment, and guarantees under current saturation tractable, allowing the use of consistent modeling and analysis approaches across fault and non-fault conditions, resembling the practices for conventional power sys-

tems. Although the proposed cross-forming implementations are promising, further research may be required to explore more advanced variants. Moreover, a comprehensive performance evaluation against grid code requirements is necessary to compare available current-limiting strategies. Furthermore, identifying the control capability boundaries of grid-forming inverters under current saturation is essential for formulating clearer and more reasonable grid-forming codes.

APPENDIX A VOLTAGE-FORMING CONTROLS: A REVIEW

A typical control block diagram for a grid-forming (voltage-forming in a narrow sense) inverter is depicted in Fig. 19. We introduce below the state-of-the-art techniques that are applied in each control module.

A. Normal Forms of Voltage-Forming Controls

Numerous voltage-forming control schemes have been developed in the literature. We categorize them into the following three major types by considering the similarities in their control architectures [7]. Notably, these controls are termed “*normal forms*” since their initial designs aim to operate as normal voltage sources without considering current saturation. Moreover, since the voltage-forming controls are mostly applied only in the positive-sequence domain, we use $\hat{v}^+ = \hat{v} \angle \hat{\theta}$ to indicate the *positive-sequence* voltage-forming reference throughout the paper.

Single-Input Single-Output Linear Type (Droop Control and Virtual Synchronous Machine): Droop control and VSMs (and their variants) are prevalent voltage-forming control schemes. Droop control and VSMs are developed with the main consideration of the nominal operating point, where the network’s power flows are reasonably approximated with decoupling and linearization. Therefore, both controls are single-input single-output (SISO), and linear in their structures. In particular, in a dominantly inductive network context, the normal form of droop control is given as

$$\dot{\hat{\theta}} = \hat{\omega} = \omega_0 + m_p(p^* - p) \quad (21a)$$

$$\hat{v} = v^* + m_q(q^* - q) \quad (21b)$$

with power droop gains $m_p \in \mathbb{R}_{\geq 0}$ and $m_q \in \mathbb{R}_{\geq 0}$, power setpoints p^* and q^* , voltage setpoint v^* , and nominal frequency

ω_0 . The power feedback p and q should be taken from positive-sequence components (i.e., calculated with positive-sequence voltage and current components; the same applies hereinafter).

Similar to droop control, VSMs have been introduced to emulate a synchronous machine electromechanical model,

$$\dot{\hat{\theta}} = \hat{\omega} \quad (22a)$$

$$T_J \dot{\hat{\omega}} = -D(\hat{\omega} - \omega_0) + (p^* - p) \quad (22b)$$

$$\hat{v} = v^* + m_q(q^* - q) \quad (22c)$$

with virtual inertia time constant T_J and damping gain D .

Multivariable and Nonlinear Type (Complex Droop Control and Dispatchable Virtual Oscillator Control): Unlike the decoupled SISO mechanism used in droop control and VSMs, “complex droop control” is structurally multivariable and nonlinear [48]. Consequently, it can effectively manage the inherent coupling and nonlinearity within the active and reactive power flows of the network. Furthermore, it performs well even when operating far from the nominal point. In polar coordinates, complex droop control reads as

$$\dot{\hat{\theta}} = \hat{\omega} = \omega_0 + \eta \left(\frac{p^*}{v^{*2}} - \frac{p}{\hat{v}^2} \right), \quad (23a)$$

$$\frac{\dot{\hat{v}}}{\hat{v}} = \hat{\varepsilon} = \eta \left(\frac{q^*}{v^{*2}} - \frac{q}{\hat{v}^2} \right) + \eta \alpha \frac{v^{*2} - \hat{v}^2}{v^{*2}} \quad (23b)$$

with power droop gain $\eta \in \mathbb{R}_{\geq 0}$ and voltage magnitude droop gain $\alpha \in \mathbb{R}_{\geq 0}$. The complex number with \hat{v}/\hat{v} as the real part and $\hat{\theta}$ as the imaginary part, i.e., $\hat{v}/\hat{v} + j\hat{\theta}$, is known as complex frequency [50]. In respect thereof, it represents both the rate of change of the voltage magnitude, $\hat{\varepsilon}$, and the angular speed, $\hat{\omega}$. This explains why (23) is termed complex droop control (complex-power complex-frequency droop control).

In complex voltage vector coordinates, complex droop control is equivalently rewritten as dispatchable virtual oscillator control (dVOC) [48],

$$\dot{\hat{v}} = j\omega_0 \hat{v} + j\eta \left(\frac{p^* - jq^*}{v^{*2}} \hat{v} - \frac{\hat{v}^+}{v^{*2}} \right) + \eta \alpha \frac{v^{*2} - \hat{v}^2}{v^{*2}} \hat{v}, \quad (24)$$

where \hat{v} is the voltage reference vector and \hat{v}_o^+ the output current (positive-sequence) [48]. It has been shown that complex droop control (i.e., dVOC) guarantees the global asymptotic stability of voltage-forming inverters in both islanded [42] and grid-connected scenarios [48].

AC-DC Dual-Port Type (Machine Matching and Dual-Port Control): Most existing voltage-forming controls focus on AC grid forming while neglecting the DC-bus voltage dynamics and regulation. To overcome this limitation, a dual-port voltage-forming control has been developed as [51]

$$\dot{\hat{\theta}} = \hat{\omega} = \omega_0 + m_p(p^* - p) + m_{dc}(v_{dc} - v_{dc}^*) \quad (25a)$$

$$\hat{v} = v^* + m_q(q^* - q), \quad (25b)$$

which regulates both the AC frequency, the AC voltage magnitude, and the DC voltage. In a particular case, $m_p = 0$, the control in (25) simplifies to a machine-matching control [52], which directly links the DC voltage to the AC frequency, reflecting a well-known observation that the DC voltage, similar to the synchronous machine frequency, indicates the power

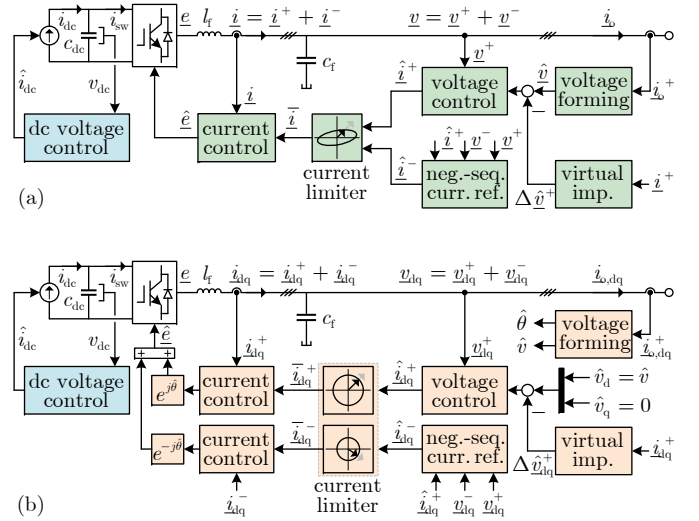


Fig. 19. Typical control diagrams of voltage-forming inverters. (a) Implementation in the stationary reference frame. (b) Implementation in the rotational reference frame. Fig. 20 displays the negative-sequence component control modes. Figs. 21 and 22 illustrates the current limiters.

imbalance of power inverters. Analogous to (25a), a hybrid-angle control is developed in [53], where a nonlinear angle-forming term is used instead of the linear active power droop, rendering a rigorous large-signal stability guarantee.

We remark that all of the voltage-forming controls shown above can be generalized to the case of resistive-inductive networks, where the power feedback should be rotated according to the network impedance angle [54].

B. Voltage Tracking or Virtual Admittance Control

Voltage Tracking Control: The inner control loops can be implemented in either the stationary or the rotational reference frame with proportional-resonant (PR) or proportional-integral (PI) regulators, respectively. We display the control implementation in stationary $\alpha\beta$ coordinates or equivalently in complex vector coordinates such as $v_\alpha + jv_\beta$ in the stationary reference frame. The counterpart in rotational dq coordinates can be obtained simply by a rotation transformation. For the former, a voltage tracking control is typically given as

$$\hat{i}^+ = \left(k_p^v + k_r^v \frac{2\omega_v s}{s^2 + 2\omega_v s + \omega_0^2} \right) (\hat{v} - \hat{v}^+), \quad (26)$$

which represents a practical PR regulator with a bandwidth of the resonant filter ω_v and control gains k_p^v and k_r^v [55].

Virtual Admittance Control: Instead of using PR or PI tracking regulators, another typical voltage control uses a virtual admittance as a proportional-like regulator [12]–[14]. A typical implementation is as follows [10]–[14],

$$\hat{i}^+ = \frac{1}{r_v + l_v s} (\hat{v} - \hat{v}^+) \quad \text{or} \quad \hat{i}^+ = \frac{1}{r_v + jx_v} (\hat{v} - \hat{v}^+) \quad (27)$$

with virtual resistance r_v and virtual inductance l_v . The voltage controller $\frac{1}{r_v + l_v s}$ functions as a dynamic virtual admittance. Alternatively, one can choose a static virtual admittance $\frac{1}{r_v + jx_v}$ [13], or even a real-valued proportional voltage control

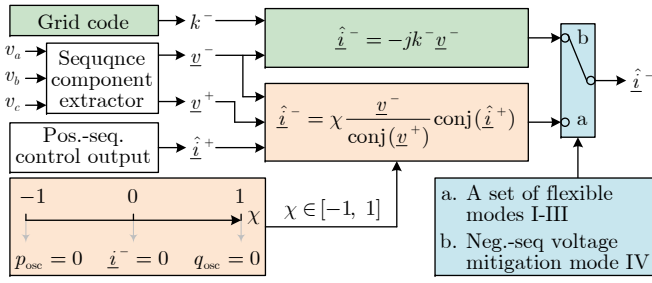


Fig. 20. Multiple control modes for negative-sequence current components. (a) A set of flexible control modes to achieve similar objectives as for conventional grid-following devices (e.g., suppressing active power or reactive power oscillation [33]); (b) Negative-sequence voltage mitigation mode (to satisfy grid code requirements) [29]. Note that these formulas apply to both $\alpha\beta$ coordinates, see the proof in Appendix B, and dq coordinates, see [28].

[12]. In a steady state, the virtual admittance control performs as a proportional gain while the PR or PI regulator tracks the voltage reference with zero errors.

C. Current Tracking Control

With a positive-sequence current reference as given in (26) and a negative-sequence current reference specified by (33) or (34) (shown in Appendix B later), the composite current reference is then given as

$$\hat{i} = \hat{i}^+ + \hat{i}^-. \quad (28)$$

Analogous to the voltage tracking control, a current tracking control in the stationary reference frame is given as

$$\hat{\underline{i}} = \left(k_p^c + k_r^c \frac{2\omega_c s}{s^2 + 2\omega_c s + \omega_0^2} \right) (\bar{\underline{i}} - \hat{\underline{i}}), \quad (29)$$

which uses a practical PR regulator with a bandwidth of the resonant filter ω_c and control gains k_p^c and k_r^c [55]. In (29), $\bar{\underline{i}}$ denotes the current reference saturated by the current limiter (introduced in Appendix C). When the current reference is not saturated, it immediately holds that $\bar{\underline{i}} = \hat{\underline{i}}$.

APPENDIX B

NEGATIVE-SEQUENCE CURRENT SPECIFICATIONS: A REVIEW OF FOUR MODES AND RIGOROUS PROOFS

For the specification of negative-sequence current references under unbalanced grid conditions, the following four modes can be typically employed.

A. Mode I: Balanced Current Control

The current of inverters is balanced when negative-sequence current components are absent. To achieve this, the negative-sequence current reference can be specified as zero, i.e.,

$$\hat{i}^- = 0. \quad (30)$$

Without providing a negative-sequence current component, the negative-sequence circuit on the inverter side is open-circuit.

B. Mode II: Active Power Oscillation Suppression

There is an oscillating component at twice the fundamental frequency in active and reactive power whenever current and voltage contain both positive- and negative-sequence components. The oscillation in either active or reactive power can be eliminated by properly specifying the negative-sequence current component. Specifically, the active power oscillation will be eliminated if and only if the negative-sequence current is given as follows [28],

$$\hat{i}^- = -\frac{v^-}{\text{conj}(v^+)} \text{conj}(\hat{i}^+), \quad (31)$$

where $\text{conj}()$ indicates a conjugate operation. In (31), the specification of the negative-sequence current reference relies on the positive-sequence current reference. The rigorous proof of (31) is given in Proposition 2 later.

C. Mode III: Reactive Power Oscillation Suppression

Similarly, the reactive power oscillation will be eliminated if and only if the negative-sequence current is given as [28],

$$\hat{i}^- = \frac{v^-}{\text{conj}(v^+)} \text{conj}(\hat{i}^+). \quad (32)$$

The proof of (32) is also given in Proposition 2.

We note that (31) and (32) are opposite, i.e., their sum is zero, reducing to (30). Hence, these modes can be synthesized as a set of *flexible modes*,

$$\hat{i}^- = \chi \frac{v^-}{\text{conj}(v^+)} \text{conj}(\hat{i}^+), \quad \chi \in [-1, 1], \quad (33)$$

where χ denotes a tunable parameter for achieving different control objectives, as illustrated in Fig. 20.

D. Mode IV: Negative-Sequence Voltage Mitigation

Alternatively, the negative-sequence current component can also be specified to suppress the negative-sequence voltage magnitude and thus improve the voltage unbalance factor (VUF). This is a requirement of grid codes. In particular, IEEE Std. 2800-2022 [30] requires that all inverter-based resources absorb negative-sequence reactive current in a proportion of the negative-sequence voltage. In respect thereof, the negative-sequence *output* current reference can be specified as

$$\hat{i}^- = -jk^- v^-, \quad (34)$$

where k^- is known as K -factor [56]. The complex coefficient jk^- relating the negative-sequence voltage to the *input* current (i.e., $-\hat{i}^- = jk^- v^-$) is equivalent to a virtual susceptance in the negative-sequence circuit, or equivalently regarded as a virtual reactance $\frac{1}{jk^-} = j(-\omega) \frac{1}{\omega k^-}$ with a negative-sequence frequency $-\omega$ and equivalent inductance $\frac{1}{\omega k^-}$. Therefore, this control mode contributes to reducing the negative-sequence voltage. A resistance/conductance component or a low-pass/band-pass filter can be incorporated into the coefficient in (34) to enhance dynamic performance.

We note that the control objectives, particularly of Modes II and III, can still be fulfilled when the positive- and negative-sequence current references are scaled down in the same ratio

by a current limiter. Furthermore, we indicate that the zero-sequence current component is inherently zero since the low-voltage-side zero-sequence circuit remains open due to the Δ -Y configuration of the step-up transformer [57].

Remark 5. Negative-Sequence Controls: GFM vs. GFL Architectures: The previous control objectives have been applied to grid-following converters for unbalanced grid conditions, which have been widely documented in the literature, see [33] for a review. Compared to the grid-following architecture, the negative-sequence current reference specification in the grid-forming architecture is largely different in Modes II and III. This is because, in the grid-following architecture, both positive- and negative-sequence current references can be flexibly specified to suppress power oscillation. In contrast, in the grid-forming architecture, only the negative-sequence current reference can be flexibly specified while the positive-sequence current reference is governed in priority by the grid-forming control. It is shown in [58] that the power oscillation suppression may also admit grid-following-like schemes, e.g., by manipulating power references and current references multiple times. However, the grid-following-like scheme is rather complicated compared to the scheme in (33).

E. A Rigorous Proof of Modes II and III

We denote positive-sequence and negative-sequence voltage and current components in complex vectors as follows: $\underline{v}^+ := v^+ e^{j\theta_v^+}$, $\underline{v}^- := v^- e^{j\theta_v^-}$, $\underline{i}^+ := i^+ e^{j\theta_c^+}$, and $\underline{i}^- := i^- e^{j\theta_c^-}$. The complex power \underline{s} is then given as

$$\begin{aligned} \underline{s} &= (\underline{v}^+ + \underline{v}^-) (\text{conj}(\underline{i}^+) + \text{conj}(\underline{i}^-)) \\ &= \underbrace{\underline{v}^+ \text{conj}(\underline{i}^+) + \underline{v}^- \text{conj}(\underline{i}^-)}_{\underline{s}_{\text{dc}}} + \underbrace{\underline{v}^+ \text{conj}(\underline{i}^-) + \underline{v}^- \text{conj}(\underline{i}^+)}_{\underline{s}_{\text{osc}}}, \end{aligned} \quad (35)$$

with a dc component $\underline{s}_{\text{dc}}$ and an oscillating component $\underline{s}_{\text{osc}}$. The oscillating component is of concern, in which the active and reactive power components are represented as

$$\begin{aligned} p_{\text{osc}} &= \underbrace{\text{Re}\{\underline{v}^+ \text{conj}(\underline{i}^-)\}}_{v^+ i^- \cos(\theta_v^+ - \theta_c^-)} + \underbrace{\text{Re}\{\underline{v}^- \text{conj}(\underline{i}^+)\}}_{v^- i^+ \cos(\theta_v^- - \theta_c^+)}, \\ q_{\text{osc}} &= \underbrace{\text{Im}\{\underline{v}^+ \text{conj}(\underline{i}^-)\}}_{v^+ i^- \sin(\theta_v^+ - \theta_c^-)} + \underbrace{\text{Im}\{\underline{v}^- \text{conj}(\underline{i}^+)\}}_{v^- i^+ \sin(\theta_v^- - \theta_c^+)}. \end{aligned} \quad (36)$$

Lemma 1. $p_{\text{osc}} = 0$ holds if and only if it holds that

$$\text{Re}\{\underline{v}^+ \text{conj}(\underline{i}^-)\} = -\text{Re}\{\underline{v}^- \text{conj}(\underline{i}^+)\}, \quad (37a)$$

$$\text{Im}\{\underline{v}^+ \text{conj}(\underline{i}^-)\} = \text{Im}\{\underline{v}^- \text{conj}(\underline{i}^+)\}. \quad (37b)$$

Similarly, $q_{\text{osc}} = 0$ holds if and only if it holds that

$$\text{Re}\{\underline{v}^+ \text{conj}(\underline{i}^-)\} = \text{Re}\{\underline{v}^- \text{conj}(\underline{i}^+)\}, \quad (38a)$$

$$\text{Im}\{\underline{v}^+ \text{conj}(\underline{i}^-)\} = -\text{Im}\{\underline{v}^- \text{conj}(\underline{i}^+)\}. \quad (38b)$$

Proof: The sufficiency is self-evident as shown in (37a) and (38a). We show below that $p_{\text{osc}} = 0$ or $q_{\text{osc}} = 0$ will also lead to (37b) or (38b), respectively.

The sine and cosine terms in (36) are functions of time t as they contain components of twice the fundamental frequency, i.e., $2\omega t$. Therefore, $p_{\text{osc}} = 0$, for any time t , leads to

$$v^+ i^- = v^- i^+, \quad \cos(\theta_v^+ - \theta_c^-) = -\cos(\theta_v^- - \theta_c^+). \quad (39)$$

Similarly, $q_{\text{osc}} = 0$, for any time t , leads to

$$v^+ i^- = v^- i^+, \quad \sin(\theta_v^+ - \theta_c^-) = -\sin(\theta_v^- - \theta_c^+). \quad (40)$$

We further show that $p_{\text{osc}} = 0$ and $q_{\text{osc}} = 0$, more specifically, (39) and (40), are mutually exclusive (cannot hold simultaneously). The proof by contradiction is as follows: (39) and (40) will lead to $\tan(\theta_v^+ - \theta_c^-) = \tan(\theta_v^- - \theta_c^+)$, and further, $\theta_v^+ - \theta_c^- = \theta_v^- - \theta_c^+ + k\pi$, $\forall k \in \mathbb{Z}$. This cannot hold for any time t since the left-hand side is a function of $2\omega t$ while the right-hand side is a function of $-2\omega t$. Hence, an accompanying result of (39) is that $\sin(\theta_v^+ - \theta_c^-) = \sin(\theta_v^- - \theta_c^+)$ while an accompanying result of (40) is that $\cos(\theta_v^+ - \theta_c^-) = \cos(\theta_v^- - \theta_c^+)$. This completes the proof of the necessity by recalling (36). ■

Proposition 2. Necessary and Sufficient Conditions for Power Non-Oscillation: Given the positive-sequence current component \underline{i}^+ , $p_{\text{osc}} = 0$ holds if and only if it holds that

$$\underline{i}^- = -\frac{\underline{v}^-}{\text{conj}(\underline{v}^+)} \text{conj}(\underline{i}^+); \quad (41)$$

Moreover, $q_{\text{osc}} = 0$ holds if and only if it holds that

$$\underline{i}^- = \frac{\underline{v}^-}{\text{conj}(\underline{v}^+)} \text{conj}(\underline{i}^+). \quad (42)$$

Proof: Consider $\underline{s}_{\text{osc}} = \underline{v}^+ \text{conj}(\underline{i}^-) + \underline{v}^- \text{conj}(\underline{i}^+)$ as in (35). By leveraging Lemma 1, it follows that $p_{\text{osc}} = 0$ holds if and only if $\underline{v}^+ \text{conj}(\underline{i}^-)$ and $\underline{v}^- \text{conj}(\underline{i}^+)$ have opposite real parts while the same imaginary parts. This is equivalent to the relationship that $\underline{v}^+ \text{conj}(\underline{i}^-) = -\text{conj}[\underline{v}^- \text{conj}(\underline{i}^+)]$, which is further equivalent to (41). In a similar vein, $q_{\text{osc}} = 0$ holds if and only if $\underline{v}^+ \text{conj}(\underline{i}^-)$ and $\underline{v}^- \text{conj}(\underline{i}^+)$ have the same real parts while opposite imaginary parts, as shown in Lemma 1. This is equivalent to $\underline{v}^+ \text{conj}(\underline{i}^-) = \text{conj}[\underline{v}^- \text{conj}(\underline{i}^+)]$ and further equivalent to (42). ■

APPENDIX C CURRENT-LIMITING STRATEGIES: A CATEGORIZED REVIEW

We consider typical existing current-limiting strategies and categorize them into three types to explicitly indicate three different technical routes to practical applications.

A. Type A: Adaptive/Threshold Virtual Impedance Control

Virtual impedance control is motivated by the requirements of reshaping the network impedance characteristics to improve dynamic performance and power-sharing [59] and by the need to limit the fault current during grid faults [8]. We introduce a fixed and an adaptive virtual impedance in the following.

A virtual impedance control module is explicitly employed to generate a voltage drop based on the current feedback [8],

$$\Delta \hat{v}^+ = (r_v + jx_v) \underline{i}^+, \quad (43)$$

where $r_v + jx_v$ denotes a virtual impedance. The voltage drop $\Delta \hat{v}^+$ is then subtracted from the voltage reference \hat{v} .

A fixed virtual impedance cannot adapt to grid fault disturbances of different severity. To overcome this limitation, a

current feedback-based adaptive virtual impedance has been proposed [8], [9], which is arranged as follows,

$$x_v = \sigma_{vi} r_v, \quad r_v = \begin{cases} 0, & |\hat{i}| \leq I_{th}, \\ \kappa_{vi} (|\hat{i}| - I_{th}), & |\hat{i}| > I_{th}, \end{cases} \quad (44)$$

where σ_{vi} is a desired X/R ratio, κ_{vi} is a proportional feedback gain, and I_{th} is a current-limiting threshold ($I_{th} < I_{lim}$). The choice of κ_{vi} is important to strictly limit the current magnitude under the maximum current. In the worst case, where a three-phase bolted fault is considered, the voltage-forming reference is canceled out completely by the virtual impedance, and κ_{vi} should satisfy that [60]

$$\begin{aligned} |\hat{v}| &\leq |\hat{i}| |r_v + jx_v| = |\hat{i}| \kappa_{vi} \sqrt{\sigma_{vi}^2 + 1} |\hat{i}| - I_{th} \\ &\leq I_{lim} \kappa_{vi} \sqrt{\sigma_{vi}^2 + 1} (I_{lim} - I_{th}), \quad (45) \\ \Rightarrow \kappa_{vi} &\geq \frac{|\hat{v}|}{I_{lim} \sqrt{\sigma_{vi}^2 + 1} (I_{lim} - I_{th})}. \end{aligned}$$

The steady-state current settles in between the threshold I_{th} and the maximum current I_{lim} in most cases where the grid fault is not a bolted fault. This implies that the maximum overcurrent capability is underutilized. To overcome this problem, a separate proportional-integral control loop has been applied in [10] and [29] to correct or estimate the ongoing voltage drop across the virtual impedance. However, this necessitates further multi-loop interaction management and parameter tuning. Moreover, it has been indicated in [22] that the X/R ratio, σ_{vi} , may need to be adaptively adjusted to reach a compromise between the damping of the current response and the margin of transient stability.

The virtual impedance strategy has been extended to more general asymmetrical fault conditions [61], [62]. In respect thereof, the 2-norm $|\hat{i}|$ cannot represent the maximum phase current magnitude. Instead, the current magnitude per phase should be detected, and the maximum phase current magnitude is used as the current feedback [61], [62].

B. Type B: Current Limiter With Virtual Admittance Control

Current saturation limiters are more intuitive for current limiting than virtual impedance emulation. Various types of current limiters have been reported in the literature, with different implementations in different coordinates, e.g., abc natural reference frame, $\alpha\beta$ stationary reference frame, and dq synchronous reference frame, as surveyed in [6]. We recall the most commonly used current limiter in the following.

1) *Current Limiter for Balanced Conditions:* When the current reference is balanced, three-phase currents have the same magnitude, which is $|\hat{i}|$. The magnitude-limited current reference, \bar{i} , is then determined by a circular limiter as

$$\bar{i} = \begin{cases} \hat{i}, & |\hat{i}| \leq I_{lim}, \\ \frac{I_{lim}}{|\hat{i}|} \hat{i}, & |\hat{i}| > I_{lim}. \end{cases} \quad (46)$$

The circular limiter is depicted in Fig. 21(a). It also directly applies to a balanced current reference in dq coordinates.

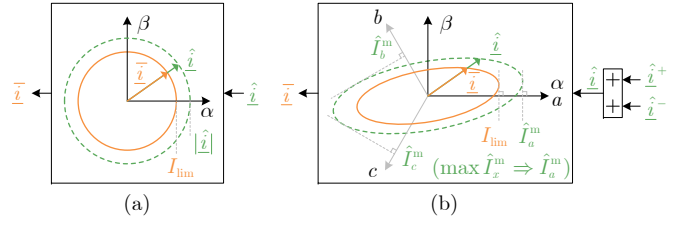


Fig. 21. Illustration of current limiters in $\alpha\beta$ coordinates. (a) Circular current limiter for balanced conditions. (b) Elliptical current limiter for unbalanced conditions.

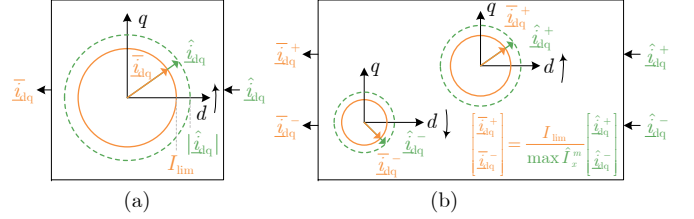


Fig. 22. Illustration of current limiters in dq coordinates. (a) Circular current limiter for balanced conditions. (b) Two circular current limiters (with equal scaling factors) for unbalanced conditions.

2) *Current Limiter for Unbalanced Conditions:* The magnitude limiting for an unbalanced current reference is not as direct as the balanced condition. The main difference is that three-phase currents have different magnitudes and the current vector, $\hat{i} = \hat{i}_\alpha + j\hat{i}_\beta$, rotates according to an ellipse rather than a circle, as illustrated in Fig. 21(b). The projection of the ellipse to each phase axis corresponds to the phase current. To avoid the overcurrent of any phase, the ellipse needs to be scaled down such that the maximum current magnitude is within the limit value. To do so, the magnitude of the phase currents needs to be identified, which is given as [27]

$$\hat{I}_x^m = \sqrt{|\hat{i}_x^+|^2 + |\hat{i}_x^-|^2 + 2 \operatorname{Re}\{\hat{i}_x^+ \hat{i}_x^- e^{j2\lambda_x}\}}, \quad (47)$$

where $x \in \{a, b, c\}$ and $\lambda_x \in \{0, -2\pi/3, 2\pi/3\}$ respectively. Based on the phase current magnitudes, the elliptical current limiter is formulated as [34], [63]

$$\bar{i} = \begin{cases} \hat{i}, & \max\{\hat{I}_a^m, \hat{I}_b^m, \hat{I}_c^m\} \leq I_{lim}, \\ \frac{I_{lim}}{\max\{\hat{I}_a^m, \hat{I}_b^m, \hat{I}_c^m\}} \hat{i}, & \max\{\hat{I}_a^m, \hat{I}_b^m, \hat{I}_c^m\} > I_{lim}. \end{cases} \quad (48)$$

Since $\hat{i} = \hat{i}^+ + \hat{i}^-$, the positive- and negative-sequence current references are scaled down equally. We notice that the limiter in (46), where $|\hat{i}| = \hat{I}_a^m = \hat{I}_b^m = \hat{I}_c^m$, is a special case of (48).

The operation of the current reference limiting in (47) and (48) can be extended to dq coordinates, i.e.,

$$\hat{I}_x^m = \sqrt{|\hat{i}_{dq}^+|^2 + |\hat{i}_{dq}^-|^2 + 2 \operatorname{Re}\{\hat{i}_{dq}^+ \hat{i}_{dq}^- e^{j2\lambda_x}\}}, \quad (49)$$

where $\hat{i}_{dq}^+ := e^{-j\hat{\theta}} \hat{i}^+$ and $\hat{i}_{dq}^- := e^{j\hat{\theta}} \hat{i}^-$ imply that $|\hat{i}_{dq}^+| = |\hat{i}^+|$, $|\hat{i}_{dq}^-| = |\hat{i}^-|$, and $\hat{i}_{dq}^+ \hat{i}_{dq}^- = \hat{i}^+ \hat{i}^-$. Accordingly, the current

limiter in dq coordinates for unbalanced cases is given as

$$\begin{bmatrix} \hat{i}_{dq}^+ \\ \hat{i}_{dq}^- \end{bmatrix} = \begin{cases} \begin{bmatrix} \hat{i}_{dq}^+ \\ \hat{i}_{dq}^- \end{bmatrix}, & \max\{\hat{i}_a^m, \hat{i}_b^m, \hat{i}_c^m\} \leq I_{\text{lim}}, \\ \frac{I_{\text{lim}}}{\max\{\hat{i}_a^m, \hat{i}_b^m, \hat{i}_c^m\}} \begin{bmatrix} \hat{i}_{dq}^+ \\ \hat{i}_{dq}^- \end{bmatrix}, & \max\{\hat{i}_a^m, \hat{i}_b^m, \hat{i}_c^m\} > I_{\text{lim}}. \end{cases} \quad (50)$$

Since \hat{i}_{dq}^+ and \hat{i}_{dq}^- are expressed in two different reference frames, the current limiter in (50) should be represented by two separate circular limiters, as illustrated in Fig. 22. One should note that the current limiter shown earlier is the most typical, but it can be extended to further improve the overcurrent capability utilization [64].

3) *Virtual Admittance Serving for Anti-Windup*: When using integrator-included (PI or PR) voltage controllers, it is necessary to configure anti-windup along with a current limiter to avoid accumulating a significant control error in the integrator during current saturation. Generally, *integrator clamping* (also known as conditional integration) and *back-calculation* (also known as tracking integration) are two standard anti-windup methods used in industry for PI [65] and PR regulators [66].

- The integrator clamping method disables the integrator whenever the output is saturated [12]. In addition, for a PR one, the resonant integrator should be reset to zero when disabled to avoid leaving a constant offset [66].
- The back-calculation method introduces a feedback loop from the portion of the output that exceeds the limiter [67], [68], reshaping the PI regulator into a lead or lag filter, and the PR regulator a band-pass or band-stop filter.

Both anti-windup methods “turn off” the integration during saturation, and afterward, the proportional regulator dominates the feedback control. In this sense, we link anti-windup with the virtual admittance control in (27), since a virtual admittance can be seen as a proportional-like regulator and does not suffer from windup. Specifically, the virtual admittance control as in (27) revises the voltage PR regulator in (26) into an equivalent admittance, shown in the following again,

$$\hat{i}^+ = \frac{1}{r_v + l_v s} (\hat{v} - v^+) \quad \text{or} \quad \hat{i}^+ = \frac{1}{r_v + jx_v} (\hat{v} - v^+). \quad (51)$$

This virtual admittance control and the virtual impedance control in (43) are equivalent in steady state when the current is unsaturated, i.e., $\hat{i}^+ = \hat{i}^+$ and $\Delta\hat{v}^+ = \hat{v} - v^+$. However, when the current is saturated, both controls lead to different equivalent impedances, see Proposition 3.

Other specific anti-windup schemes for voltage-forming inverters include: adjusting the outer-loop active and reactive power reference [39], limiting the outer-loop voltage and power reference [69], applying a virtual impedance to reduce the voltage reference [63], moving the current limiter to the outer layer of voltage-forming controls [27], [70], etc.

C. Type C: Saturated-Current-Forming Control

During current saturation, it is also possible to deactivate or bypass the voltage control and solely maintain the current control. This thus falls into the scope of current-forming control,

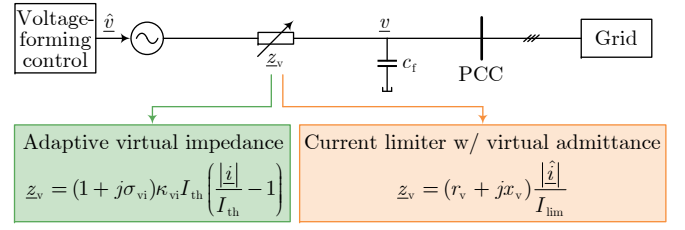


Fig. 23. A unified equivalent circuit representation [71] for both the adaptive virtual impedance control [8], [9] and the current limiter with virtual admittance control [10]–[14], where the resulting equivalent impedance is current-dependent for both current-limiting strategies.

as described in Definition 2 and Table I. In this respect, the reference angle of the current vector control can be generated by a PLL or an angle-forming control, e.g., $\dot{\theta} = \omega_0 + k_p(p^* - p)$. Based on the latter, many recent studies have explored directly specifying current references (in dq coordinates) during current saturation [15]–[19], where various stabilizing remedies have been developed, such as using the q-axis voltage feedback [15] and adjusting the current reference angle [16]–[18]. Since this control belongs to the current-forming type, the source under forming is current rather than voltage. In other words, the voltage-forming functionality cannot be maintained by this current-forming control mode.

D. Unified Equivalent Circuit for Type-A and -B Strategies

A unified equivalent circuit has been established to describe the output behavior of voltage-forming inverters with an activated adaptive virtual impedance or an activated current limiter with a virtual admittance [71]. Concerning a balanced condition, the unified circuit is reformulated precisely in the following Proposition 3. The result can also be extended to unbalanced conditions, where the circuit refers to the positive-sequence domain.

Proposition 3. Unified and Current-Dependent Equivalent Circuit: Consider a voltage-forming inverter under current saturation, where either the adaptive virtual impedance in (44) or the current limiter in (46) alongside the virtual admittance in (51) is activated. The output behavior of the voltage-forming inverter can be represented by a unified equivalent circuit in Fig. 23, where the equivalent virtual impedance z_v is dependent on the current \hat{i} or its reference \hat{i} , respectively, as follows,

$$z_v = (1 + j\sigma_{vi})\kappa_{vi}I_{th} \left(\frac{|\hat{i}|}{I_{th}} - 1 \right), \quad (52)$$

$$z_v = (r_v + jx_v) \frac{|\hat{i}|}{I_{\text{lim}}}. \quad (53)$$

Proof: First, we consider the adaptive virtual impedance in (44), which is derived as

$$\begin{aligned} z_v &= r_v + jx_v = (1 + j\sigma_{vi})\kappa_{vi}(|\hat{i}| - I_{th}) \\ &= (1 + j\sigma_{vi})\kappa_{vi}I_{th} \left(\frac{|\hat{i}|}{I_{th}} - 1 \right). \end{aligned} \quad (54)$$

This completes the proof of (52). Next, we consider the current limiter in (46) and the virtual admittance in (51) (with a static

admittance) for balanced conditions and arrive at

$$\begin{aligned}\hat{v} - \underline{v} &= \hat{i}(r_v + jx_v) = \frac{\hat{i}}{I_{\text{lim}}} (r_v + jx_v) \bar{i} \\ &= \underbrace{\frac{\hat{i}}{I_{\text{lim}}} (r_v + jx_v)}_{z_v} \bar{i},\end{aligned}\quad (55)$$

where it is assumed that the output current \hat{i} tracks the saturated reference \bar{i} . The proof of (53) is completed. ■

The fact that the resulting virtual impedance for current limiting is current-dependent is reasonable since a larger equivalent impedance is required to limit a higher overcurrent. On the other hand, this implies that the equivalent virtual impedance is unpredictable, depending on the fault current which is influenced by the fault severity. It has been found in [12]–[14] that the current-dependent equivalent impedance leads to a distorted power-angle relationship. Moreover, the unpredictable virtual impedance brings significant difficulties in transient stability analysis and insufficient robustness to unforeseen fault disturbances. When using the developed cross-forming control in this work, the virtual internal voltage magnitude proves to be current-dependent while the virtual impedance is constant, making transient stability analysis tractable.

The unified equivalent circuit establishes a connection between the two independently developed current-limiting strategies. However, this does not suggest that both strategies provide the same performance. The most significant difference is that the saturated current in using the adaptive virtual impedance locates in between I_{th} and I_{lim} , whereas the saturated current in using the current limiter locates at I_{lim} . More comparisons can be found in Table II.

REFERENCES

- [1] A. Johnson, "Minimum specification required for provision of GB grid forming (GBGF) capability (formerly virtual synchronous machine/VSM capability)," 2021. [Online]. Available: <https://www.nationalgrideso.com/industry-information/codes/gc/modifications/gc0137-minimum-specification-required-provision-gb-grid>
- [2] "Voluntary specification for grid-forming inverters," Australian Energy Market Operator (AEMO), Tech. Rep., 2023.
- [3] B. Bahrani, M. H. Ravanji, B. Kroposki, D. Ramasubramanian, X. Guillaud, T. Prevost, and N.-A. Cutululis, "Grid-forming inverter-based resource research landscape: Understanding the key assets for renewable-rich power systems," *IEEE Power Energy Mag.*, vol. 22, no. 2, pp. 18–29, 2024.
- [4] D. Pan, X. Wang, F. Liu, and R. Shi, "Transient stability of voltage-source converters with grid-forming control: A design-oriented study," *IEEE J. Emerg. Sel. Top. Power Electron.*, vol. 8, no. 2, pp. 1019–1033, 2020.
- [5] R. Rosso, X. Wang, M. Liserre, X. Lu, and S. Engelken, "Grid-forming converters: Control approaches, grid-synchronization, and future trends—a review," *IEEE Open J. Ind. Appl.*, vol. 2, pp. 93–109, 2021.
- [6] H. Zhang, W. Xiang, W. Lin, and J. Wen, "Grid forming converters in renewable energy sources dominated power grid: Control strategy, stability, application, and challenges," *J. Mod. Power Syst. Clean Energy*, vol. 9, no. 6, pp. 1239–1256, 2021.
- [7] F. Dörfler and D. Groß, "Control of low-inertia power systems," *Annu. Rev. Control Robot. Auton. Syst.*, vol. 6, pp. 415–445, 2023.
- [8] A. D. Paquette and D. M. Divan, "Virtual impedance current limiting for inverters in microgrids with synchronous generators," *IEEE Trans. Ind. Appl.*, vol. 51, no. 2, pp. 1630–1638, 2015.
- [9] T. Qoria, F. Gruson, F. Colas, X. Kestelyn, and X. Guillaud, "Current limiting algorithms and transient stability analysis of grid-forming VSCs," *Electr. Power Syst. Res.*, vol. 189, p. 106726, 2020.
- [10] R. Rosso, S. Engelken, and M. Liserre, "On the implementation of an FRT strategy for grid-forming converters under symmetrical and asymmetrical grid faults," *IEEE Trans. Ind. Appl.*, vol. 57, no. 5, pp. 4385–4397, 2021.
- [11] K. V. Kkuni and G. Yang, "Effects of current limit for grid forming converters on transient stability: analysis and solution," *Int. J. Electr. Power Energy Syst.*, vol. 158, p. 109919, 2024.
- [12] B. Fan and X. Wang, "Equivalent circuit model of grid-forming converters with circular current limiter for transient stability analysis," *IEEE Trans. Power Syst.*, vol. 37, no. 4, pp. 3141–3144, 2022.
- [13] Y. Zhang, C. Zhang, R. Yang, M. Molinas, and X. Cai, "Current-constrained power-angle characterization method for transient stability analysis of grid-forming voltage source converters," *IEEE Trans. Energy Convers.*, vol. 38, no. 2, pp. 1338–1349, 2023.
- [14] K. G. Saffar, S. Driss, and F. B. Ajaei, "Impacts of current limiting on the transient stability of the virtual synchronous generator," *IEEE Trans. Power Electron.*, vol. 38, no. 2, pp. 1509–1521, 2023.
- [15] L. Huang, H. Xin, Z. Wang, L. Zhang, K. Wu, and J. Hu, "Transient stability analysis and control design of droop-controlled voltage source converters considering current limitation," *IEEE Trans. Smart Grid*, vol. 10, no. 1, pp. 578–591, 2019.
- [16] E. Rokrok, T. Qoria, A. Bruyere, B. Francois, and X. Guillaud, "Transient stability assessment and enhancement of grid-forming converters embedding current reference saturation as current limiting strategy," *IEEE Trans. Power Syst.*, vol. 37, no. 2, pp. 1519–1531, 2022.
- [17] Y. Liu, H. Geng, M. Huang, and X. Zha, "Dynamic current limiting of grid-forming converters for transient synchronization stability enhancement," *IEEE Trans. Ind. Appl.*, pp. 1–11, 2023.
- [18] Y. Li, Y. Lu, J. Yang, X. Yuan, R. Yang, S. Yang, H. Ye, and Z. Du, "Transient stability of power synchronization loop based grid forming converter," *IEEE Trans. Energy Convers.*, pp. 1–16, 2023.
- [19] G. Wang, L. Fu, Q. Hu, C. Liu, and Y. Ma, "Transient synchronization stability of grid-forming converter during grid fault considering transient switched operation mode," *IEEE Trans. Sustain. Energy*, vol. 14, no. 3, pp. 1504–1515, 2023.
- [20] H. Xin, K. Zhuang, P. Hu, Y. Gu, and P. Ju, "Dual synchronous generator: Inertial current source based grid-forming solution for VSC," *arXiv preprint arXiv:2107.01805*, 2021.
- [21] M. Schweizer, S. Almer, S. Pettersson, A. Merkert, V. Bergemann, and L. Harnefors, "Grid-forming vector current control," *IEEE Trans. Power Electron.*, vol. 37, no. 11, pp. 13 091–13 106, 2022.
- [22] T. Qoria, H. Wu, X. Wang, and I. Colak, "Variable virtual impedance-based overcurrent protection for grid-forming inverters: Small-signal, large-signal analysis and improvement," *IEEE Trans. Smart Grid*, vol. 14, no. 5, pp. 3324–3336, 2023.
- [23] T. Liu, X. Wang, F. Liu, K. Xin, and Y. Liu, "A current limiting method for single-loop voltage-magnitude controlled grid-forming converters during symmetrical faults," *IEEE Trans. Power Electron.*, vol. 37, no. 4, pp. 4751–4763, 2022.
- [24] T. Qoria, F. Gruson, F. Colas, G. Denis, T. Prevost, and X. Guillaud, "Critical clearing time determination and enhancement of grid-forming converters embedding virtual impedance as current limitation algorithm," *IEEE J. Emerg. Sel. Top. Power Electron.*, vol. 8, no. 2, pp. 1050–1061, 2020.
- [25] Y. Li, Y. Gu, and T. C. Green, "Revisiting grid-forming and grid-following inverters: A duality theory," *IEEE Trans. Power Syst.*, vol. 37, no. 6, pp. 4541–4554, 2022.
- [26] Y. Zhang, C. Zhang, M. Molinas, and X. Cai, "Control of virtual synchronous generator with improved transient angle stability under symmetric and asymmetric short circuit fault," *IEEE Trans. Energy Convers.*, 2024.
- [27] M. A. Awal, M. R. K. Rachi, H. Yu, I. Husain, and S. Lukic, "Double synchronous unified virtual oscillator control for asymmetrical fault ride-through in grid-forming voltage source converters," *IEEE Trans. Power Electron.*, vol. 38, no. 6, pp. 6759–6763, 2023.
- [28] T. Zheng, L. Chen, Y. Guo, and S. Mei, "Flexible unbalanced control with peak current limitation for virtual synchronous generator under voltage sags," *J. Mod. Power Syst. Clean Energy*, vol. 6, no. 1, pp. 61–72, 2018.
- [29] M.-A. Nasr and A. Hooshyar, "Controlling grid-forming inverters to meet the negative-sequence current requirements of the IEEE Standard 2800-2022," *IEEE Trans. Power Del.*, vol. 38, no. 4, pp. 2541–2555, 2023.
- [30] IEEE Standards Association, "IEEE standard for interconnection and interoperability of inverter-based resources (IBRs) interconnecting with associated transmission electric power systems," *IEEE Std. 2800-2022*, pp. 1–180, 2022.

- [31] X. He, C. He, S. Pan, H. Geng, and F. Liu, "Synchronization instability of inverter-based generation during asymmetrical grid faults," *IEEE Trans. Power Syst.*, vol. 37, no. 2, pp. 1018–1031, 2022.
- [32] X. He, H. Geng, J. Xi, and J. M. Guerrero, "Resynchronization analysis and improvement of grid-connected VSCs during grid faults," *IEEE J. Emerg. Sel. Top. Power Electron.*, vol. 9, no. 1, pp. 438–450, 2021.
- [33] J. Jia, G. Yang, and A. H. Nielsen, "A review on grid-connected converter control for short-circuit power provision under grid unbalanced faults," *IEEE Trans. Power Del.*, vol. 33, no. 2, pp. 649–661, 2018.
- [34] I. Sadeghkhani, M. E. Hamedani Golshan, J. M. Guerrero, and A. Mehrizi-Sani, "A current limiting strategy to improve fault ride-through of inverter interfaced autonomous microgrids," *IEEE Trans. Smart Grid*, vol. 8, no. 5, pp. 2138–2148, 2017.
- [35] H. Wu and X. Wang, "Small-signal modeling and controller parameters tuning of grid-forming vscs with adaptive virtual impedance-based current limitation," *IEEE Trans. Power Electron.*, vol. 37, no. 6, pp. 7185–7199, 2022.
- [36] O. Mo, S. D'Arco, and J. A. Suul, "Evaluation of virtual synchronous machines with dynamic or quasi-stationary machine models," *IEEE Trans. Ind. Electron.*, vol. 64, no. 7, pp. 5952–5962, 2017.
- [37] J. Alipoor, Y. Miura, and T. Ise, "Power system stabilization using virtual synchronous generator with alternating moment of inertia," *IEEE J. Emerg. Sel. Top. Power Electron.*, vol. 3, no. 2, pp. 451–458, 2015.
- [38] H. Wu and X. Wang, "A mode-adaptive power-angle control method for transient stability enhancement of virtual synchronous generators," *IEEE J. Emerg. Sel. Top. Power Electron.*, vol. 8, no. 2, pp. 1034–1049, 2020.
- [39] M. G. Taul, X. Wang, P. Davari, and F. Blaabjerg, "Current limiting control with enhanced dynamics of grid-forming converters during fault conditions," *IEEE J. Emerg. Sel. Top. Power Electron.*, vol. 8, no. 2, pp. 1062–1073, 2020.
- [40] J. Wang and X. Zhang, "Active power and voltage cooperative control for improving fault ride-through capability of grid-forming converters," *IEEE Trans. Ind. Electron.*, pp. 1–11, 2024.
- [41] J. Schiffer, R. Ortega, A. Astolfi, J. Raisch, and T. Sezi, "Conditions for stability of droop-controlled inverter-based microgrids," *Automatica*, vol. 50, no. 10, pp. 2457–2469, 2014.
- [42] M. Colombino, D. Groß, J.-S. Brouillon, and F. Dörfler, "Global phase and magnitude synchronization of coupled oscillators with application to the control of grid-forming power inverters," *IEEE Trans. Autom. Control*, vol. 64, no. 11, pp. 4496–4511, 2019.
- [43] X. He and F. Dörfler, "Passivity and decentralized stability conditions for grid-forming converters," *IEEE Trans. Power Syst.*, pp. 1–4, 2024.
- [44] M. Choopani, S. H. Hosseinian, and B. Vahidi, "New transient stability and LVRT improvement of multi-VSG grids using the frequency of the center of inertia," *IEEE Trans. Power Syst.*, vol. 35, no. 1, pp. 527–538, 2020.
- [45] Z. Shuai, C. Shen, X. Liu, Z. Li, and Z. J. Shen, "Transient angle stability of virtual synchronous generators using Lyapunov's direct method," *IEEE Trans. Smart Grid*, vol. 10, no. 4, pp. 4648–4661, 2019.
- [46] M. Kabalan, P. Singh, and D. Niebur, "Large signal Lyapunov-based stability studies in microgrids: A review," *IEEE Trans. Smart Grid*, vol. 8, no. 5, pp. 2287–2295, 2017.
- [47] P. Kundur, *Power System Stability and Control*. New York, NY, USA: McGraw Hill, 1994.
- [48] X. He, L. Huang, I. Subotić, V. Häberle, and F. Dörfler, "Quantitative stability conditions for grid-forming converters with complex droop control," *IEEE Trans. Power Electron.*, pp. 1–19, 2024.
- [49] M. A. Desai, X. He, L. Huang, and F. Dörfler, "Saturation-informed current-limiting control for grid-forming converters," *Electr. Power Syst. Res.*, pp. 1–7, 2023.
- [50] F. Milano, "Complex frequency," *IEEE Trans. Power Syst.*, vol. 37, no. 2, pp. 1230–1240, 2022.
- [51] I. Subotić and D. Groß, "Power-balancing dual-port grid-forming power converter control for renewable integration and hybrid AC/DC power systems," *IEEE Trans. Control Netw. Syst.*, vol. 9, no. 4, pp. 1949–1961, 2022.
- [52] L. Huang, H. Xin, Z. Wang, K. Wu, H. Wang, J. Hu, and C. Lu, "A virtual synchronous control for voltage-source converters utilizing dynamics of DC-link capacitor to realize self-synchronization," *IEEE J. Emerg. Sel. Top. Power Electron.*, vol. 5, no. 4, pp. 1565–1577, 2017.
- [53] A. Tayyebi, A. Anta, and F. Dörfler, "Grid-forming hybrid angle control and almost global stability of the DC-AC power converter," *IEEE Trans. Autom. Control*, vol. 68, no. 7, pp. 3842–3857, 2023.
- [54] J. C. Vasquez, J. M. Guerrero, A. Luna, P. Rodriguez, and R. Teodorescu, "Adaptive droop control applied to voltage-source inverters operating in grid-connected and islanded modes," *IEEE Trans. Ind. Electron.*, vol. 56, no. 10, pp. 4088–4096, 2009.
- [55] D. Zmood and D. Holmes, "Stationary frame current regulation of PWM inverters with zero steady-state error," *IEEE Trans. Power Electron.*, vol. 18, no. 3, pp. 814–822, 2003.
- [56] VDE/FNN, "Technical requirements for the connection and operation of customer installations to the high voltage network (TAR high voltage)," 2017.
- [57] Ö. Göksu, R. Teodorescu, C. L. Bak, F. Iov, and P. Carne Kjær, "Impact of wind power plant reactive current injection during asymmetrical grid faults," *IET Renew. Power Gener.*, vol. 7, no. 5, pp. 484–492, 2013.
- [58] S. Pola, M. Azzouz, A. S. Awad, and H. Sindi, "Fault ride-through strategies for synchronverter-interfaced energy resources under asymmetrical grid faults," *IEEE Trans. Sustain. Energy*, vol. 14, no. 4, pp. 2391–2405, 2023.
- [59] A. S. Vijay, N. Parth, S. Doolla, and M. C. Chandorkar, "An adaptive virtual impedance control for improving power sharing among inverters in islanded ac microgrids," *IEEE Trans. Smart Grid*, vol. 12, no. 4, pp. 2991–3003, 2021.
- [60] B. Fan, T. Liu, F. Zhao, H. Wu, and X. Wang, "A review of current-limiting control of grid-forming inverters under symmetrical disturbances," *IEEE Open J. Power Electron.*, vol. 3, pp. 955–969, 2022.
- [61] N. Baekeland, D. Venkatramanan, M. Kleemann, and S. Dhople, "Stationary-frame grid-forming inverter control architectures for unbalanced fault-current limiting," *IEEE Trans. Energy Convers.*, vol. 37, no. 4, pp. 2813–2825, 2022.
- [62] H. Zhang, R. Liu, C. Xue, and Y. Li, "Simultaneous overvoltage and overcurrent mitigation strategy of grid-forming inverters under a single-line-to-ground fault," *IEEE Trans. Ind. Electron.*, 2023.
- [63] S. F. Zarei, H. Mokhtari, M. A. Ghasemi, and F. Blaabjerg, "Reinforcing fault ride through capability of grid forming voltage source converters using an enhanced voltage control scheme," *IEEE Trans. Power Del.*, vol. 34, no. 5, pp. 1827–1842, 2019.
- [64] K. Schönleber, E. Prieto-Araujo, S. Ratés-Palau, and O. Gomis-Bellmunt, "Extended current limitation for unbalanced faults in MMC-HVDC-connected wind power plants," *IEEE Trans. Power Del.*, vol. 33, no. 4, pp. 1875–1884, 2018.
- [65] J.-W. Choi and S.-C. Lee, "Antiwindup strategy for PI-type speed controller," *IEEE Trans. Ind. Electron.*, vol. 56, no. 6, pp. 2039–2046, 2009.
- [66] A. Ghoshal and V. John, "Anti-windup schemes for proportional integral and proportional resonant controller," in *National Power Electronic Conference*, 2010.
- [67] O. Ajala, M. Lu, B. Johnson, S. V. Dhople, and A. Domínguez-García, "Model reduction for inverters with current limiting and dispatchable virtual oscillator control," *IEEE Trans. Energy Convers.*, vol. 37, no. 4, pp. 2250–2259, 2022.
- [68] H. Zhang, R. Liu, C. Xue, and Y. Li, "Active power enhancement control strategy of grid-forming inverters under asymmetrical grid faults," *IEEE Trans. Power Electron.*, vol. 39, no. 1, pp. 1447–1459, 2023.
- [69] J. Chen, F. Prystupczuk, and T. O'Donnell, "Use of voltage limits for current limitations in grid-forming converters," *CSEE J. Power Energy Syst.*, vol. 6, no. 2, pp. 259–269, 2020.
- [70] S. Jiang, Y. Zhu, T. Xu, and G. Konstantinou, "Current-synchronization control of grid-forming converters for fault current limiting and enhanced synchronization stability," *IEEE Trans. Power Electron.*, pp. 1–15, 2024.
- [71] H. Wu, X. Wang, and L. Zhao, "Design considerations of current-limiting control for grid-forming capability enhancement of VSCs under large grid disturbances," *IEEE Trans. Power Electron.*, pp. 1–5, 2024.